

Distribution Agreement

In presenting this thesis or dissertation as a partial fulfillment of the requirements for an advanced degree from Emory University, I hereby grant to Emory University and its agents the non-exclusive license to archive, make accessible, and display my thesis or dissertation in whole or in part in all forms of media, now or hereafter known, including display on the world wide web. I understand that I may select some access restrictions as part of the online submission of this thesis or dissertation. I retain all ownership rights to the copyright of the thesis or dissertation. I also retain the right to use in future works (such as articles or books) all or part of this thesis or dissertation.

DocuSigned by:
Signature: 
0C5963369DBD425...

Hannah Lute
Name

10/12/2023 | 5:34 PM EDT
Date

Title Structural and Functional Characterization of the Asprosin and Protein Tyrosine Phosphatase Receptor Type D (PTPRD) Interaction

Author Hannah Lute

Degree Master of Science

Program Biological and Biomedical Sciences
Biochemistry, Cell and Developmental Biology

Approved by the Committee

DocuSigned by:

523BA27634FF4E6...

Eric Ortlund
Advisor

DocuSigned by:

0E321480F386404...

Michael Koval
Committee Member

DocuSigned by:

4DDA20DAD30547B...

Nicholas Seyfried
Committee Member

Committee Member

Committee Member

Committee Member

Accepted by the Laney Graduate School:

Kimberly Jacob Arriola, Ph.D, MPH
Dean, James T. Laney Graduate School

Date

Structural and Functional Characterization of the Asprosin and Protein Tyrosine Phosphatase Receptor Type D (PTPRD) Interaction

By

Hannah Lute

B.S. Grand Valley State University, 2021

Advisor: Eric Ortlund, PhD

An abstract of

A thesis submitted to the Faculty of the

James T. Laney School of Graduate Studies of Emory University

in partial fulfillment of the requirements for the degree of

Masters of Science in Graduate Division of Biomedical Sciences,

Biochemistry, Cell, and

Developmental Biology.

2023

Abstract

Structural and Functional Characterization of the Asprosin and Protein Tyrosine Phosphatase Receptor Type D (PTPRD) Interaction

By: Hannah Lute

By the year 2030, 50% of Americans are expected to be obese. Difficulty in treating obesity comes from an inability to control appetite and modulate hepatic glucose release in patients. A hormone, named asprosin, was recently discovered to stimulate an increase in appetite through its interaction with the protein tyrosine phosphatase receptor type D (PTPRD) in the hypothalamus. This interaction has considerable potential as a therapeutic target that can be harnessed to treat obesity through modulation of appetite. The goal of this project is to characterize the asprosin-PTPRD complex structurally and functionally as a basis for future pharmacological design.

Structural and Functional Characterization of the Asprosin and Protein Tyrosine Phosphatase Receptor Type D (PTPRD) Interaction

By

Hannah Lute

B.S. Grand Valley State University, 2021

Advisor: Eric Ortlund, PhD

A thesis submitted to the Faculty of the
James T. Laney School of Graduate Studies of Emory University
in partial fulfillment of the requirements for the degree of
Masters of Science in Graduate Division of Biomedical Sciences,
Biochemistry, Cell, and
Developmental Biology.

2023

Table of Contents

Chapter One: Regulation of Appetite Through the Melanocortin System..... 1

Introduction:	1
The melanocortin system and appetite regulation	1
Agouti-related protein (AgRP)/ Neuropeptide Y (NPY)-expressing neurons.....	2
Proopiomelanocortin (POMC)-expressing neurons	2
Key players: leptin, insulin, and ghrelin	3
Asprosin, a new player in the game	5
Figures	6
Figure 1.1: Opposing actions of AgRP and POMC neurons within the ARH.....	6
Figure 1.2: Mechanisms of hormone signaling in the melanocortin system.	7
References.....	8

Chapter Two: Expression and Purification of Asprosin..... 11

Introduction	11
Results	12
Bacterial Expression Constructs	12
Mammalian Expression Constructs.....	18
Discussion.....	22
Bacterial Expression Constructs	22
Mammalian Expression Constructs.....	23
Figures	25
Figure 2.1: Asprosin in pET-28a(+) test expressions.....	25
Table 2.1: Dialysis conditions for stepwise refold of asprosin from inclusion bodies.	26
Figure 2.2: Asprosin inclusion body stepwise refold.....	27
Figure 2.3: Alphafold generated model of asprosin.....	28
Figure 2.4: Nickel affinity purification of truncated asprosin cleavable MBP construct.	29
Figure 2.5: Post-TEV cleavage of truncated asprosin cleavable MBP construct.....	30
Figure 2.6: SEC of truncated asprosin cleavable MBP post-TEV protease cleavage.....	31
Figure 2.7: Amylose-affinity purification of truncated asprosin rigid MBP construct.....	32
Figure 2.8: Test expressions of truncated asprosin MBP-fusion constructs co-expressed with molecular chaperones.....	33
Figure 2.9: Validation of truncated asprosin cleavable MBP expression with molecular chaperones.	34

Figure 2.10: Purification of truncated asprosin with cleavable MBP from molecular chaperone co-expression.	35
Figure 2.11: Expression of asprosin-pLVX mammalian expression construct.	36
Table 2.2: Primers used for amplification and addition of Gibson arms to asprosin fragment.	37
Figure 2.12: Mammalian expression of full-length (FL) asprosin Fc-fusion and Truncated (Trunc) asprosin Fc-fusion.	38
.....	39
Figure 2.13: Purification of asprosin Fc-fusion constructs using nickel-affinity chromatography.....	39
Figure 2.14: Asprosin-Fc fusion representations.....	40
Materials and Methods.....	41
Asprosin in pET-28a(+)	41
Refolding asprosin from inclusion bodies	41
Mammalian Expression.....	43
References.....	44
Chapter Three: Expression and Purification of Protein Tyrosine Phosphatase Receptor Type D (PTPRD).....	46
Introduction	46
Results	48
PTPRD Domains.....	48
Full-Length PTPRD Extracellular Domain	48
Crystallizable PTPRD.....	49
Discussion.....	50
Figures.....	52
Table 3.1: Primers used for generation of PTPRD Expression Plasmids.	52
Figure 3.1: PTPRD Truncation Expression Plasmids.	53
Figure 3.2: Purification scheme for PTPRD-Fn.	54
Figure 3.3: Purification Scheme of PTPRD-IgG.	55
Figure 3.4: Purity of PTPRD domains following size-exclusion chromatography.	56
Table 3.2: Primers used for generation of crystallizable PTPRD construct.....	57
Figure 3.5: PCR amplification of crystallizable PTPRD.	58
Materials and Methods.....	59
Cloning	59
Protein Expression and Purification	60
References.....	63

Chapter Four: Characterization of the Asprosin-PTPRD Interaction.....	66
Introduction	66
Results	67
Negative Stain Electron Microscopy	67
Cryogenic Electron Microscopy.....	68
Bio-Layer Interferometry.....	68
Discussion.....	69
Figures	72
Figure 4.1: Reconstruction of the PTPRD-asprosin complex by negative-stain EM.	72
Figure 4.2: 2D Classes of the Asprosin-PTPRD Complex.	73
Figure 4.3: Binding Kinetics of Asprosin and full-length extracellular domain of PTPRD Determined Using BLI.....	74
Methods/Materials	75
Negative Stain Electron Microscopy	75
Cryogenic Electron Microscopy.....	75
Bio-Layer Interferometry.....	76
References.....	77
Chapter Five: Future Considerations for the Asprosin Project.....	78
Deep Mutational Scanning.....	78
Site-Directed Mutagenesis	79
Asprosin Clinical Trial	80
Placensin and Gonascin	80
Figure 5.1: Multiple sequence alignment of asprosin and IL1RAPL1.....	82
Figure 5.2: Sandwich ELISA used for plasma asprosin detection.	83
Figure 5.3: 3D modeling of asprosin, placensin, and gonascin.	84
References.....	85

Chapter One: Regulation of Appetite Through the Melanocortin System

Introduction:

The melanocortin system and appetite regulation

Understanding exactly how appetite is modulated within the brain has been of growing interest over the past decade. Obesity has reached an epidemic level, with over 1.9 billion adults being affected according to the World Health Organization. Unfortunately, this prevalence is only expected to grow. By the year 2030 it is expected that 50% of Americans will be obese (1). Appetite stimulation is an important concept to understand, as it could have pharmacological potential in regard to the treatment and prevention of obesity. Current knowledge of the mechanism behind appetite regulation revolves around the melanocortin system, which is a complex set of signaling pathways that are made up of five G-protein coupled melanocortin receptors, peptide agonists derived from the proopiomelanocortin prohormone precursor; and the endogenous antagonists, agouti and agouti-related protein (2). Aside from its role in appetite regulation and feeding behaviors, the physiological roles of the melanocortin system are extensive, including pigmentation, adrenocortical steroidogenesis, energy homeostasis, natriuresis, erectile responses, energy homeostasis, and exocrine gland secretion (2). The melanocortin system involves two distinct neuronal populations within the arcuate nucleus of the hypothalamus (ARH), Agouti-related protein (AgRP)/ Neuropeptide Y (NPY)-expressing neurons and proopiomelanocortin (POMC)-expressing neurons (3). AgRP/NPY-expressing neurons are referred to as being orexigenic, or appetite stimulating, while POMC-expressing neurons work to inhibit appetite (3). Melanocortin neurons are responsible for the appetite regulation role of this system by regulating the release of endogenous melanocortin ligands by sensing and integrating neuronal and hormonal signals (4).

The five sub-types of melanocortin receptors (Mcr) include Mc1r, Mc2r, Mc3r, Mc4r, and Mc5r. The Mcr receptors are 7 transmembrane G-protein coupled receptors of the rhodopsin family (5). Mc3r and Mc4r are the receptors that are primarily expressed in the brain, with Mc4r specifically playing a major role in energy homeostasis (5). Mc4r is activated or inhibited by the melanocortin ligands which have an overall effect of increasing or reducing food intake, as well as increasing or decreasing energy expenditure (5).

Agouti-related protein (AgRP)/ Neuropeptide Y (NPY)-expressing neurons

AgRP/NPY-expressing neurons are a distinct neuronal population that are located exclusively within the ARH. AgRP neurons are located in close proximity to the median eminence (6), which is a region of the brain where the blood brain barrier is not fully formed and is particularly permissive, allowing neurons access to circulating hormones and nutrients (7). Aside from AgRP, AgRP neurons also express neuropeptide Y (NPY) and gamma-aminobutyric acid (GABA) (6). AgRP, NPY, and GABA are released into the paraventricular nucleus (PVN) of the hypothalamus, which directly antagonizes Mc3R and Mc4R to stimulate feeding behaviors (**Figure 1.1**) (6). Actions of the AgRP neurons are in direct opposition to the actions of the POMC neurons. The balance of the actions of these neuronal populations is crucial for proper energy homeostasis.

Proopiomelanocortin (POMC)-expressing neurons

Activation of the Proopiomelanocortin (POMC)- expressing neurons is through hormonal signals responsible for reducing feeding behaviors and increasing energy expenditure (2). Similarly to AgRP neurons, POMC neurons are also located in close proximity to the median eminence. Post-feeding signaling events lead to increased expression and processing of POMC into mature α -melanocyte-stimulating hormone (α -

MSH) (3). POMC neurons project into the PVN of the hypothalamus, which is where they release α -MSH, the natural agonist of Mc4r, causing a decrease in food seeking behaviors, while simultaneously causing an increase in energy expenditure (**Figure 1.1**) (3).

Key players: leptin, insulin, and ghrelin

While the majority of signaling related to appetite stimulation and energy expenditure occurs via signaling cascades within the neuronal populations of the ARH, it is important to tease apart the molecular mechanisms of the hormonal signals that initiate these cascades. The hormones that have been well characterized within this system include leptin, insulin and ghrelin. When thinking of hormones within the context of the melanocortin system, many associate leptin with POMC expressing hormones, and ghrelin with AgRP/NPY expressing neurons; however, it is important to note that while these hormones play excitatory roles in this distinct way, they simultaneously play inhibitory roles for the opposing neuronal population (4). For instance, while leptin's main role is to activate POMC neurons, leptin additionally binds to leptin receptors on the surface of AgRP/NPY expressing neurons to inhibit expression of AgRP and NPY (7).

Ghrelin is released from the stomach to stimulate appetite in times of fasting (8). Of the hormonal pathways involved in this study, the ghrelin signaling pathway is the least understood. The mechanism by which ghrelin stimulates appetite in the hypothalamus is unique from the mechanisms of insulin and leptin in that it does not alter mRNA levels of AgRP/NPY or POMC, but instead it increases the firing of AgRP neurons (9). The receptor for ghrelin in the hypothalamus is a G-protein coupled receptor on the surface of AgRP neurons termed GHS-R1 (9). It has been proposed that ghrelin stimulates appetite by

modulating synaptic plasticity (9). Synaptic plasticity is an activity-dependent modification of the strength or efficacy of synaptic transmission at preexisting synapses (10). Ghrelin's role in synaptic plasticity is likely due to mobilization of intracellular calcium stores via activation of the phospholipase C (PLC) pathway (**Figure 1.2**) (9). The changes in synaptic plasticity have the overall effect of increasing the firing rate of AgRP neurons and decreasing the firing of POMC neurons, and subsequently increasing appetite.

Insulin controls expression of melanocortin ligands by controlling induction and repression of forkhead box O-class 1 (FoxO1) (5). FoxO1 is a transcription factor, responsible for the transcription of the *Agrp* gene, which causes expression of the AgRP peptide (11). FoxO1 regulates expression of *Agrp* and *Pomc* by competing with signal transducer and activator of transcription 3 (STAT3) for their promoter sites (12). FoxO1 activates the *Agrp* promoter, and simultaneously inhibits the *Pomc* promoter. In a fasted state, FoxO1 is located at the nucleus of both POMC and AgRP neurons (11). Following feeding, insulin binds to insulin receptors on AgRP and POMC neurons, which causes activation of Phosphoinositide 3 (PI-3) Kinase. This kinase subsequently activates the serine/threonine kinase, Akt, which phosphorylates FoxO1, inducing translocation to the cytoplasm. Translocation of FoxO1 to the cytoplasm downregulates its activity, causing a decrease in AgRP peptide production, leading to a decrease in appetite (**Figure 1.2**) (11).

Leptin is released into the circulatory system following feeding from adipose tissue. Leptin has been shown to upregulate expression of POMC and downregulate AgRP through the Janus kinase-signal transducer and activator of transcription (JAK2-STAT3) pathway (13). Following feeding, leptin binds to leptin receptors on the surface of POMC neurons. Leptin receptors in the hypothalamus contain several JAK2 binding sites.

Following leptin binding, JAK2 phosphorylates STAT3. Phosphorylated STAT3 travels to the nucleus where it competes with FoxO1 to increase transcription of *Pomc* and decrease transcription of *Agrp* (Figure 1.2) (13). This has an overall effect of decreasing appetite.

Asprosin, a new player in the game

Recent studies revealed that asprosin, an orexigenic (appetite stimulating) hormone that originates from white adipose tissue (14), acts by interacting with the protein tyrosine phosphatase receptor type D (PTPRD) in the ARH (15). However, how asprosin modulates PTPRD activity to promote appetite stimulation remains unknown. The main goals of this study aim to understand the asprosin-PTPRD interaction with the long-term goal of understanding how this interaction fits into the melanocortin system as a whole. The asprosin-PTPRD interaction has potential as a pharmacological target to treat obesity through modulation of appetite. POMC expression through the JAK2-STAT3 pathway is of particular interest for this study due to the presence of STAT3 in AgRP/NPY expressing neurons, as well as its direct interaction with PTPRD (16). Recent studies have shown that asprosin decreases STAT3 phosphorylation through interaction with PTPRD (15). This finding is significant because it places asprosin within the same signaling cascades as leptin and insulin, providing another possible avenue for appetite stimulation independent of ghrelin signaling. The goal of this project is to understand the interaction between asprosin and its receptor, PTPRD in the hypothalamus, and how this interaction may fit within the overall paradigm of appetite regulation.

Figures

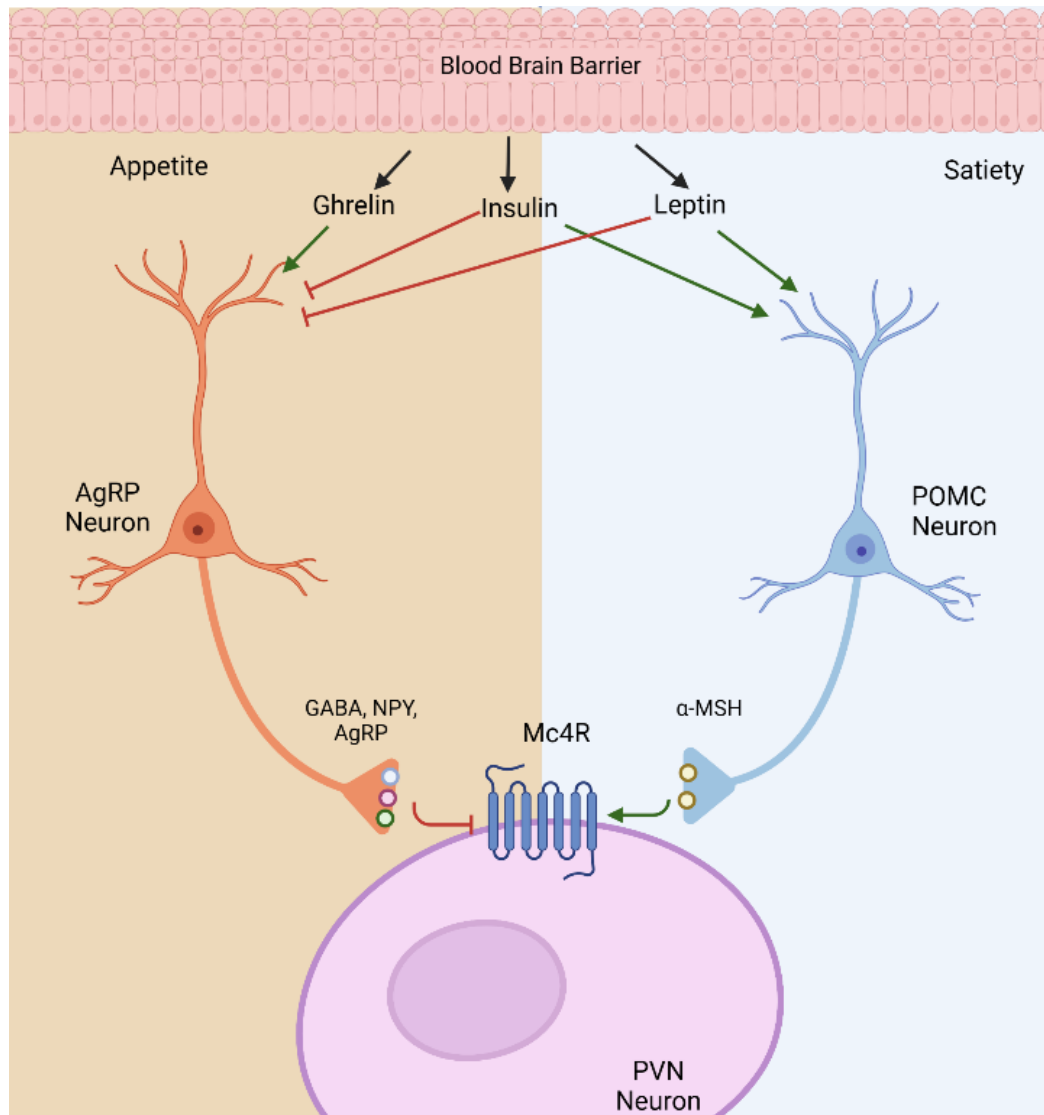


Figure 1.1: Opposing actions of AgRP and POMC neurons within the ARH. AgRP and POMC neurons compete with each other for activation or inhibition of Mc4R to regulate appetite and energy expenditure. AgRP and POMC neurons respond to hormonal signals from ghrelin, insulin and leptin. Figure created using BioRender.

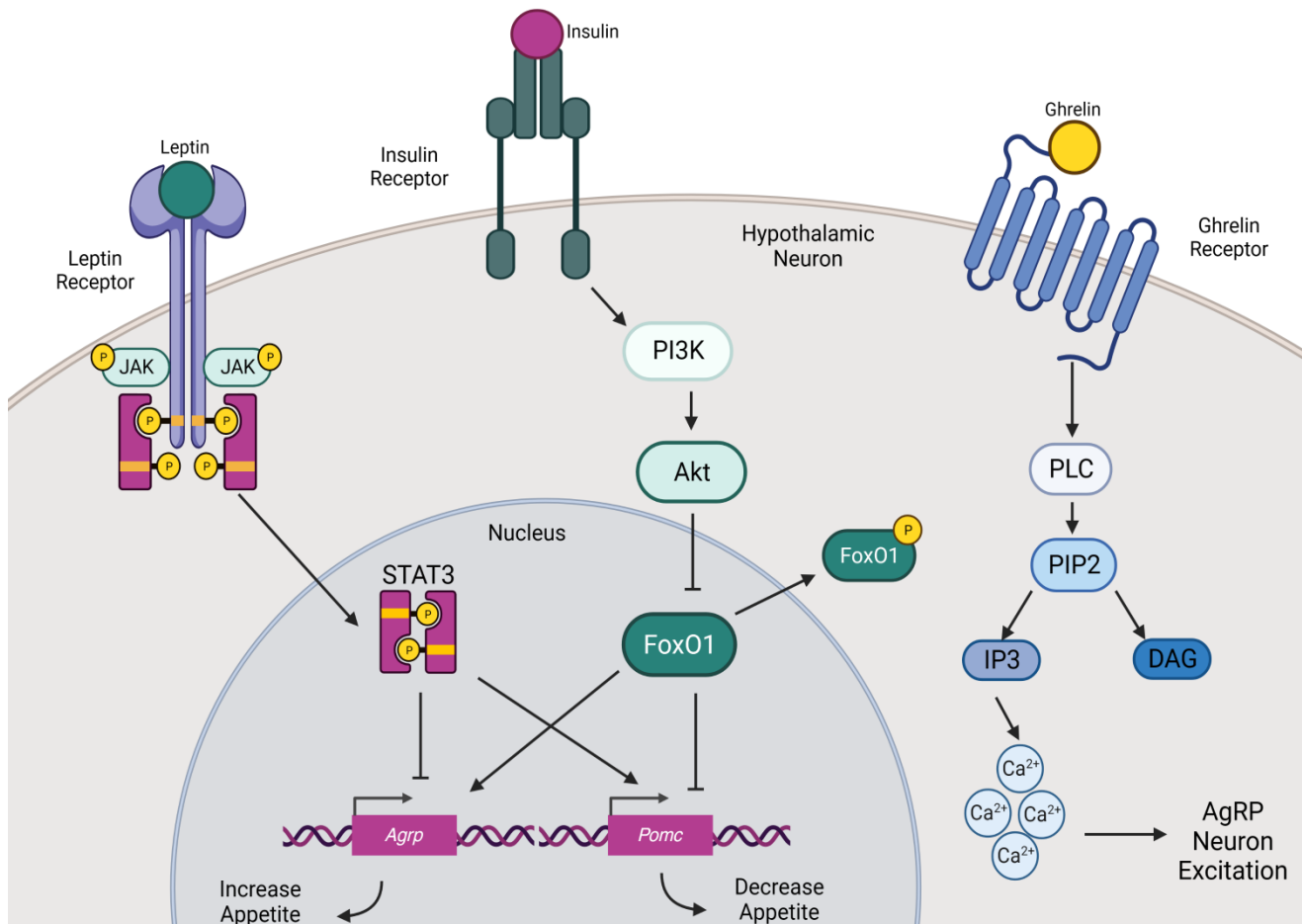


Figure 1.2: Mechanisms of hormone signaling in the melanocortin system. Leptin, insulin and ghrelin initiate signaling cascades within the ARH to regulate appetite. Insulin and leptin act by altering mRNA levels of melanocortin ligands, AgRP and POMC. Ghrelin acts to mobilize intracellular calcium stores and increase AgRP neuron firing. Figure created using BioRender.

References

1. Ward ZJ, Bleich SN, Cradock AL, Barrett JL, Giles CM, Flax C, Long MW, Gortmaker SL. Projected U.S. State-Level Prevalence of Adult Obesity and Severe Obesity. *New England Journal of Medicine*. 2019;381(25):2440-50. doi: 10.1056/NEJMsa1909301. PubMed PMID: 31851800.
2. Cone RD. Studies on the Physiological Functions of the Melanocortin System. *Endocrine Reviews*. 2006;27(7):736-49. doi: 10.1210/er.2006-0034.
3. Sohn JW. Network of hypothalamic neurons that control appetite. *BMB Rep*. 2015;48(4):229-33. Epub 2015/01/07. doi: 10.5483/bmbrep.2015.48.4.272. PubMed PMID: 25560696; PMCID: PMC4436859.
4. Yang Y, Xu Y. The central melanocortin system and human obesity. *J Mol Cell Biol*. 2020;12(10):785-97. Epub 2020/09/26. doi: 10.1093/jmcb/mjaa048. PubMed PMID: 32976556; PMCID: PMC7816681.
5. Williams KW, Scott MM, Elmquist JK. Modulation of the central melanocortin system by leptin, insulin, and serotonin: co-ordinated actions in a dispersed neuronal network. *Eur J Pharmacol*. 2011;660(1):2-12. Epub 2011/01/08. doi: 10.1016/j.ejphar.2010.11.042. PubMed PMID: 21211525; PMCID: PMC3085544.
6. Deem JD, Faber CL, Morton GJ. AgRP neurons: Regulators of feeding, energy expenditure, and behavior. *Febs j*. 2022;289(8):2362-81. Epub 2021/09/02. doi: 10.1111/febs.16176. PubMed PMID: 34469623; PMCID: PMC9040143.
7. Morita-Takemura S, Wanaka A. Blood-to-brain communication in the hypothalamus for energy intake regulation. *Neurochem Int*. 2019;128:135-42. Epub 2019/04/20. doi: 10.1016/j.neuint.2019.04.007. PubMed PMID: 31002894.

8. Abizaid A, Horvath TL. Ghrelin and the central regulation of feeding and energy balance. *Indian J Endocrinol Metab.* 2012;16(Suppl 3):S617-26. Epub 2013/04/09. doi: 10.4103/2230-8210.105580. PubMed PMID: 23565498; PMCID: PMC3602992.
9. Ibrahim Abdalla MM. Ghrelin - Physiological Functions and Regulation. *Eur Endocrinol.* 2015;11(2):90-5. Epub 2015/08/01. doi: 10.17925/ee.2015.11.02.90. PubMed PMID: 29632576; PMCID: PMC5819073.
10. Citri A, Malenka RC. Synaptic Plasticity: Multiple Forms, Functions, and Mechanisms. *Neuropsychopharmacology.* 2008;33(1):18-41. doi: 10.1038/sj.npp.1301559.
11. Sasaki T, Kitamura T. Roles of FoxO1 and Sirt1 in the central regulation of food intake. *Endocr J.* 2010;57(11):939-46. Epub 2010/11/05. doi: 10.1507/endocrj.k10e-320. PubMed PMID: 21048357.
12. Cao Y, Nakata M, Okamoto S, Takano E, Yada T, Minokoshi Y, Hirata Y, Nakajima K, Iskandar K, Hayashi Y, Ogawa W, Barsh GS, Hosoda H, Kangawa K, Itoh H, Noda T, Kasuga M, Nakae J. PDK1-Foxo1 in agouti-related peptide neurons regulates energy homeostasis by modulating food intake and energy expenditure. *PLoS One.* 2011;6(4):e18324. Epub 2011/06/23. doi: 10.1371/journal.pone.0018324. PubMed PMID: 21694754; PMCID: PMC3072380 the study. There are no employment or consultancy issues and no patents, products in development or marketed products to declare. The authors also confirm that this does not alter their adherence to all the PLoS ONE policies on sharing data and materials.
13. Ernst MB, Wunderlich CM, Hess S, Paehler M, Mesaros A, Korolov SB, Kleinridders A, Husch A, Münzberg H, Hampel B, Alber J, Kloppenburg P, Brüning JC,

Wunderlich FT. Enhanced Stat3 activation in POMC neurons provokes negative feedback inhibition of leptin and insulin signaling in obesity. *J Neurosci.* 2009;29(37):11582-93. Epub 2009/09/18. doi: 10.1523/jneurosci.5712-08.2009. PubMed PMID: 19759305; PMCID: PMC6665760.

14. Romere C, Duerrschmid C, Bournat J, Constable P, Jain M, Xia F, Saha PK, Del Solar M, Zhu B, York B, Sarkar P, Rendon DA, Gaber MW, LeMaire SA, Coselli JS, Milewicz DM, Sutton VR, Butte NF, Moore DD, Chopra AR. Asprosin, a Fasting-Induced Glucogenic Protein Hormone. *Cell.* 2016;165(3):566-79. Epub 2016/04/19. doi: 10.1016/j.cell.2016.02.063. PubMed PMID: 27087445; PMCID: PMC4852710.

15. Mishra I, Xie WR, Bournat JC, He Y, Wang C, Silva ES, Liu H, Ku Z, Chen Y, Erokwu BO, Jia P, Zhao Z, An Z, Flask CA, He Y, Xu Y, Chopra AR. Protein tyrosine phosphatase receptor δ serves as the orexigenic asprosin receptor. *Cell Metab.* 2022;34(4):549-63.e8. Epub 2022/03/18. doi: 10.1016/j.cmet.2022.02.012. PubMed PMID: 35298903; PMCID: PMC8986618.

16. Kim M, Morales LD, Jang IS, Cho YY, Kim DJ. Protein Tyrosine Phosphatases as Potential Regulators of STAT3 Signaling. *Int J Mol Sci.* 2018;19(9). Epub 2018/09/14. doi: 10.3390/ijms19092708. PubMed PMID: 30208623; PMCID: PMC6164089.

Chapter Two: Expression and Purification of Asprosin

Introduction

Asprosin is a recently discovered glucogenic and orexigenic hormone, stimulating appetite and hepatic glucose release, respectively (1). Asprosin falls within a class of hormones known as protein hormones. Canonically, protein hormones are cleaved from larger pro-proteins and circulate to have a physiological effect on a target organ via interactions with cell surface receptors (2). Asprosin is encoded within exons 65 and 66 of the *FBN1* gene, which also encodes for fibrillin (1). Fibrillin is an extracellular connective tissue protein that is a structural component that contributes to the overall structure of a microfibril (3). Fibrillin is initially expressed as a pro-peptide (profibrillin) which is processed into fibrillin and asprosin via a Furin cleavage at the C-terminal end of profibrillin. Asprosin is the last 140 amino acids of the C-terminal end and is approximately 30 kDa due to three predicted N-linked glycosylation sites (1). Asprosin originates in white adipose tissue and travels to several tissues to carry out its function, such as the liver and the hypothalamus.

Asprosin was initially discovered in studies of patients with a condition known as neonatal progeroid syndrome (NPS). Symptoms of NPS include elongated limbs, elongated facial features, lean stature, and lack of feeding behaviors. In many cases, the lack of feeding behaviors caused patients to be malnourished. Samples from NPS patients were taken and analyzed with Sanger sequencing and whole-exome sequencing to look for patterns in mutations that would culminate in NPS symptoms (1). The initial experiment included 5 patients with NPS. Sequencing revealed that all of these patients had mutations in the C-terminal region of *FBN1*, either right before the Furin cleavage site, or after the cleavage site. All of these mutations resulted in the loss

of the C-terminal cleavage product, which we now recognize as asprosin (1). Interest in asprosin is not only contained to its context within NPS, but within the larger context of obesity and metabolic health. Due to its implications in regulating appetite through its interaction within the hypothalamus (4), there is hope that this interaction could be targeted pharmacologically, to be used as a future treatment for obesity through modulation of appetite. Prior characterization of this interaction has been minimal, and extensive experiments are needed to understand this interaction both functionally and structurally, which is the goal of this work.

The Ortlund lab is looking to complement the previous *in vivo* work done by the Chopra lab at Case Western Reserve University with *in vitro* structural characterization and biochemical assays. The first step in this process is to produce and purify asprosin in amounts that are adequate for characterization techniques. This has proven to be the most challenging component of this study. While some of the methods for expression and purification of asprosin have been successful in producing some protein, a method to produce large quantities is still desired.

Results

Bacterial Expression Constructs

Asprosin was initially received in a mammalian adenoviral expression plasmid from the Chopra group used for *in vivo* studies. A bacterial expression plasmid was desirable, as bacterial expression is often able to generate more protein, in a quicker, less-expensive effort. As mentioned previously, asprosin contains three N-linked glycosylation sites within its sequence. While bacteria are not able to achieve some post-translational modifications, such as glycosylation, we were hopeful that the non-glycosylated version of asprosin may be able to be expressed, and that glycosylation is not important for this

interaction, therefore causing non-glycosylated asprosin to behave in biochemical assays in the same way as glycosylated asprosin.

Asprosin in pET-28a(+)

The first effort to express asprosin in bacteria was in a general, commonly used bacterial expression vector, pET-28a(+). Asprosin was cloned into the pET-28a(+) vector with a 6X-histidine tag (his-tag) located on the N-terminus of asprosin for nickel-affinity chromatography. Asprosin-pET-28a was expressed in *Escherichia coli* BL21 (DE3) cells. Test expressions were performed in small-scale cultures with a variety of conditions, to optimize expression. The first condition that was altered was expression media, small scale cultures were inoculated in either Luria broth (LB) or terrific broth (TB). Each media condition was also tested with day growths (four hours) or overnight growths. Expression was induced using different concentrations of isopropyl- β -d-1-thiogalactopyranoside (IPTG). Samples of each growth condition were collected pre and post induction with IPTG. Pre and post samples were analyzed on a 12% SDS-PAGE gel (**Fig. 2.1**). It was not clear from test expression what optimal expression conditions were for this construct, as there did not seem to be good expression for any of the conditions. However, following day growth conditions there was noticeable presence of inclusion bodies.

Refolding asprosin from inclusion bodies

A research group from Guangxi Medical University in China indicated that they were able to obtain pure, biologically active asprosin from bacteria through inclusion body denaturation and refolding (5). Due to presence of inclusion bodies resulting from day growths, this seemed like a viable next direction to move in for asprosin expression and purification, if soluble protein was not able to be obtained.

The same asprosin-pET-28a construct expressed in *E. coli* BL21 (DE3) cells was used to produce inclusion bodies. Cultures were inoculated into LB and grown to an OD₆₀₀ of 0.8 and induced with a final concentration of 0.5 mM IPTG at 37 °C for four hours. Following growth, cell mass was collected using centrifugation. Cells were lysed using sonication on ice. Following sonication and centrifugation, there were large inclusion bodies present.

Inclusion bodies were washed using a 1 M urea and 1% sodium cholate solution. Three washes were performed to remove excess cellular debris and inclusion bodies were dissolved in buffer containing 8M urea, EDTA, and Tris. Following unfolding, total protein concentration was measured and adjusted to 1 mg/mL using 8M urea. Protein was refolded using a stepwise refolding method, slowly dialyzing out urea from 8M to 0M over a two-day time period (**Table 2.1**). Following dialysis, protein was further purified and concentrated by nickel-affinity chromatography. A gradient elution scheme with imidazole was used to elute the refolded protein from the nickel column. However, the protein did not elute at a specific imidazole concentration, and the elution profile spanned over the entirety of the chromatogram. Fractions from nickel-affinity chromatography were analyzed on a 12% SDS-PAGE gel, which indicated pure protein at approximately 15 kDa, the expected size of non-glycosylated asprosin (**Figure 2.2**).

To validate that the refolded protein was the expected size of asprosin, I used size exclusion chromatography (SEC). I concentrated the refolded protein to a final volume of 100 μ L and injected it onto an Enrich 70 sepharose column. The chromatogram showed a small peak eluting at the expected volume. However, when this fraction was analyzed

on a 12% SDS-PAGE gel, it became evident that the protein was rapidly degrading (**Fig. 2.2**).

AlphaFold modeling of asprosin

While asprosin has not been able to be produced in a large enough quantity to study its structure experimentally through x-ray crystallography or cryo-EM, we have begun to examine the predicted structure of asprosin using AlphaFold, which is an artificial intelligence-based structure prediction and modeling software. AlphaFold works by jointly embedding multiple sequence alignments (MSAs) and pairwise features, a new output representation and associated loss to enable accurate end-to-end structure prediction (6).

Asprosin's amino acid sequence was fed into AlphaFold 2 collab and the standard parameters were used to generate a 3D model. The model of asprosin is highly confident with only a small, disordered region where the predicted structure is not as confident. The structure of asprosin resembles an Ig-fold with three glycosylation sites. Two of the three glycosylation sites are predicted to be located within the disordered N-terminal region (**Fig. 2.3**).

Truncated asprosin

Since two of asprosin's three glycosylation sites were predicted to be located in the disordered N-terminal region of asprosin, we wondered if a truncated version of asprosin with this disordered region removed, would be more readily expressed in bacteria. Two constructs of asprosin were designed with the first 20 amino acid residues removed. The first construct contained truncated asprosin with an N-terminal his-tag followed by a C-terminal maltose binding protein (MBP), which is a commonly used protein to aid in protein solubility. The first construct contained a TEV protease cleavage

site, so that the his-tag and MBP may be removed for future binding and structural studies. The second truncated asprosin construct also contained an N-terminal MBP tag, however this construct contained a rigid linker in between the MBP tag and asprosin. This construct also lacked a 6X histidine tag and a TEV site. The second construct was designed in case cleavage of the MBP tag caused protein degradation. These constructs were ordered and synthesized by Twist Biosystems.

Similarly to the initial expression construct of full-length asprosin in pET28-a(+), I began analyzing the expression capabilities of the truncated constructs by running small-scale test expressions in a variety of conditions. I began by working with the truncated asprosin construct with the cleavable MBP. LB and TB expression media were tested, day growths and overnight growths, as well as different concentrations of IPTG for induction. Samples of each condition were taken and analyzed using a 12% SDS-PAGE gel and a western blot was done using an anti-his HRP conjugated antibody to look for presence of his-tagged protein. The western blot indicated presence of his-tagged protein coordinating to the expected size of truncated asprosin (~13 kDa) (Data not shown). The greatest amount of protein was observed in overnight growths in TB media. IPTG concentration did not seem to affect expression levels.

Since test expression with the cleavable construct was viable, I scaled up growth to 3 liters. Cultures were grown to an $OD_{600} = 0.8$ and induced with a final concentration of 300 mM IPTG overnight at 16 °C. Cell mass was collected by centrifugation, resuspended, and lysed using sonication on ice. Cleavable-MBP-truncated-asprosin was initially purified using nickel-affinity chromatography. Fractions containing cleavable-MBP-truncated-asprosin were identified by SDS-PAGE (**Fig. 2.4**), pooled and dialyzed

against buffer containing 1 mg TEV protease. Following TEV protease cleavage, the tagged MBP was removed by an additional Nickel-affinity column (**Fig. 2.5**). The flowthrough containing cleavable-MBP-truncated-asprosin was concentrated using an Amicon Ultra 10K centrifugal filter device (Millipore), concentrated to 5.6 mg/mL. The final purity of cleavable-MBP-truncated-asprosin was assessed using SDS-PAGE. Following TEV cleavage of MBP, the protein of expected size was no longer present (**Fig. 2.6**). It is possible that the MBP tag was required for stabilization, and removal facilitated protein precipitation or degradation.

Non-cleavable-MBP-truncated-asprosin was purified using amylose affinity with a gravity column. Samples were collected from pre-induction with IPTG, post induction, flow-through, buffer wash, and sample and assessed by SDS-PAGE. There was no protein of the expected size (~55 kDa) present (**Fig. 2.7**).

Chaperone Proteins

Due to lack of ability of to produce soluble protein and difficulty refolding protein from inclusion bodies, we decided co-express asprosin with different molecular chaperone proteins. Molecular chaperones are a ubiquitous group of proteins which mediate the correct folding of other proteins (7). There are several different molecular chaperones and co-chaperones that function in ATP-coordinated cycles of binding and release from folding intermediates to suppress off-pathway aggregation and facilitate proper folding of proteins in *E. coli* (8). The chaperones explored in this project were trigger factor (tig), DnaK/DnaJ/GrpE and GroES/GroEL. Five different chaperone system constructs, each containing different combinations of the systems mentioned previously, were co-expressed with the truncated asprosin cleavable MBP construct and the

truncated asprosin rigid linker MBP (non-cleavable) construct in *E. coli* BL21 (DE3) cells. Small-scale cultures were grown in LB to an OD₆₀₀ of 0.6. The chaperones were induced first with their designated inducers for one hour at 37 °C. Following induction of the chaperone systems, the asprosin constructs were induced with 500 μM IPTG at 16°C overnight. Expression of asprosin was assessed by SDS-PAGE and western blot. The presence of his-tagged protein of approximately 55 kDa was observed for the cleavable MBP construct (**Fig. 2.8, Fig. 2.9**). SDS-PAGE indicated that there was protein of the correct size present from the non-cleavable construct, however this construct does not contain a his-tag, so it is unclear if this is truly the MBP-asprosin fusion (**Fig. 2.10**). Chaperone systems that contained trigger factor produced the most amount of protein of the correct size.

In order for the co-expression with chaperone systems to be an effective way to produce asprosin for structural studies, we need to be able to purify asprosin away from the chaperone proteins following expression. To do this we used nickel-affinity chromatography and size-exclusion chromatography. While we were able to purify asprosin away from most of the chaperone proteins, the protein degraded rapidly following purification (**Fig. 2.11**).

Mammalian Expression Constructs

Efforts to achieve bacterial expression of asprosin did not produce promising results, therefore efforts turned to mammalian expression. Glycosylation is achievable in mammalian cells, so we were hopeful that this would lead to production of asprosin in amounts needed for structural studies.

Asprosin in PAH

A mammalian expression vector had been produced by University of North Carolina Chapel Hill's Protein Expression & Purification and Macromolecular Crystallography (PEP-MX) Core Lab. PAH vector is a fairly common mammalian expression plasmid that can be used to generate a stable cell line using adenovirus. We received this plasmid and began to test expression in Expi293 suspension cells (ThermoFisher Scientific), which are optimized for protein expression.

Prior to transfection, Expi293 cells were expanded and passaged three times. Cells were grown to a final concentration according to the recommendations of the manufacturer. A complex of plasmid DNA and ExpiFectamine transfection reagent was made and incubated at room temperature for 15 minutes. Following incubation, the transfection complex was added to the 125 mL flask dropwise. Cells were incubated at 37 °C with a humidified atmosphere of 8% CO₂. Twenty-four hours after transfection, transfection enhancers were added to the cells. Following the addition of the enhancers, cells began to die rapidly. It appeared that asprosin was toxic to cells. Samples were taken from the media and from the cells and analyzed them using SDS-PAGE (data not shown). It was evident that the protein was staying within the cells and was not being secreted into the media. Whole plasmid sequencing of the construct revealed that the construct did not contain a secretion sequence. Consequently, asprosin stayed within the cells, causing them to die.

Asprosin in pLVX

It became clear that a secretion sequence was necessary for optimal mammalian expression of asprosin. I decided to sub-clone asprosin from the PAH construct from UNC into a vector previously used in the Ortlund Lab, known as pLVX. pLVX was the vector of

choice due to its utility in producing lenti-virus and ability to generate a stable cell line. A construct of asprosin was designed that contained the asprosin sequence along with an N-terminal IL2 leader sequence for secretion. The asprosin fragment was amplified and the addition of Gibson arms complementary to the pLVX plasmid, as well as the addition of the IL2 sequence were carried out via polymerase chain reaction (**Table 2.2**). Gibson assembly was used to produce the asprosin-pLVX construct and this was confirmed using whole plasmid sequencing. The Expi293 system (ThermoFisher Scientific) was the mammalian expression system selected for expression of this construct.

Prior to transfection, Expi293 cells were expanded and passaged three times. Cells were grown to a final concentration of 5.6 million cells/mL and then diluted in a 125 mL flask to 3.0 million cells/mL. A complex of plasmid DNA and ExpiFectamine transfection reagent was made and incubated at room temperature for 15 minutes. Following incubation, the transfection complex was added to the 125 mL flask dropwise. Cells were incubated at 37 °C with a humidified atmosphere of 8% CO₂. Twenty-four hours after transfection, transfection enhancers were added to the cells.

Three days after transfection, cells were harvested, and media was separated from the cells by centrifugation. The cell media was then purified using nickel affinity chromatography by FPLC (BioRad). The chromatogram from nickel affinity revealed a small protein peak. Samples from the peak were assessed using SDS-PAGE, where no protein bands were visible. Peak fractions were collected and concentrated to 300 µL with a final concentration of 0.453 mg/mL. Concentrated fractions were assessed with SDS-PAGE and a western blot. An anti asprosin antibody was used to detect asprosin. Purchased asprosin was used as a control for the western blot. There was no indication

of asprosin in the media, but the band corresponding to purchased asprosin was visualized (**Fig. 2.12**).

Asprosin Fc-fusion

Interest in asprosin as a pharmacological treatment for patients with NPS inspired design of a construct that contains asprosin as an Fc fusion protein. Fc fusion proteins are composed of an immunoglobulin Fc domain that is directly linked to another peptide (9). Fc-fusion proteins are most often expressed as homodimers and are commonly used due to several biological and pharmacological benefits that come with having the Fc domain present (9). Fc domain folds have been shown previously to improve the solubility and stability of the fusion protein partner, which is highly desirable in this project considering the extensive efforts pursued to obtain soluble asprosin. In a pharmacological sense, presence of an Fc domain can increase the plasma half-life of the fusion protein partner, which consequently prolongs the therapeutic activity of the associated protein (9). A concern for this project is whether or not the Fc fusion protein will have the capability to cross the blood brain barrier. We are optimistic that an asprosin Fc-fusion would have the ability to cross the blood brain barrier as asprosin crosses the blood brain barrier at the most permissive region (median eminence) and previous studies have shown that an Fc-fusion was able to cross the blood brain barrier (10).

A construct of asprosin with an Fc domain attached on the C-terminus was designed and produced by Twist Biosystems. Two different constructs were designed, a full-length asprosin construct and a truncated asprosin construct. The final asprosin Fc construct consists of a secretion signal, histidine tagged asprosin followed by a six amino acid linker composed of glycine residues, and the Fc fusion protein expressed on the C-

terminal end. The Expi293 expression system (ThermoFisher Scientific) was used to transfect cells with the asprosin-Fc constructs. Samples from each transfection (both from the cells and media) were collected, and added to buffer that either contained reducing agent or didn't contain reducing agent (**Fig. 2.13**). The purpose of running each sample with or without reducing agent is to see if the Fc fusion is forming a homodimer as it should. Samples were run on a 12% SDS-PAGE gel and analyzed by western blot using a mouse His-Tag antibody HRP conjugate (Novagen). The western blot showed presence of his-tagged protein resulting from both constructs, however there was no difference between the samples in reducing versus non-reducing conditions.

Since the western blot revealed that his-tagged protein was present in the media of the transfections I proceeded with purification of this protein. I collected the media from each transfection and purified it using nickel-affinity chromatography. I collected fractions and assessed protein purity using a 12% SDS-PAGE gel and a western blot with a mouse His-Tag antibody HRP conjugate (Novagen) to look for his-tagged protein. The expected size of asprosin with the Fc fusion protein is approximately 65 kDa, which was evident on the SDS-PAGE gel. However, the western blot only indicated his-tagged protein in the fractions from the truncated asprosin construct. There also seemed to be significant protein degradation (**Fig. 2.13**).

Discussion

Bacterial Expression Constructs

Bacterial expression of asprosin does not produce protein amounts needed for structural studies. However, bacterial constructs can yield large inclusion bodies that contain asprosin. Denaturation and refolding of this protein has the potential to yield

substantial amounts of pure protein. Stepwise refolding methods require optimization. The stepwise protocol described produced substantial amounts of protein; however, this was not easily replicated, and the protein degraded rapidly. Substantial protein crash out was observed as the protocol proceeded into the later steps. To maximize protein yield, a faster refold method may be best in order to limit the amount of crash out. Future efforts for protein refolding should be centered around using a fast-dilution method or an on-column based method for refolding to avoid the stepwise refolding method. A faster refold method may also be easier to replicate. The stepwise refolding method described has been replicated three times. Of the three times, refolded protein was only obtained two times. Protein stability also will need to be addressed in order for this method to be successful. In both of the times where refolded protein was obtained, the protein was not able to be assessed properly, as it degraded rapidly. The second trial of this refolding method included a substantial amount of different protease inhibitors, to try and prevent protein degradation. However, the addition of these components did not change the fate of the protein.

Mammalian Expression Constructs

Similarly to bacterial expression, it seems that it is difficult to express asprosin even within a mammalian expression system. The most promising avenue of mammalian asprosin expression seems to be an Fc-fusion asprosin construct. This is the only construct thus far where his-tagged protein is carried all the way through purification. However, the protein degrades very rapidly following purification. There also seems to be an issue with formation of the Fc-homodimer, as indicated by the lack of change in size following treatment with reducing agent. Formation of the homodimer is important, as this is the active state of the Fc protein, which is required in order to have the effect of

increasing plasma half-life. To combat this issue in the future, there should be several different Fc-fusion constructs designed, each with a different length of glycine linker in between asprosin and the Fc protein. It is possible that flexibility within this linker is enabling asprosin to interfere with Fc dimerization. Efforts should be made to find the optimal linker length to allow for dimerization to occur. Another interesting avenue for an Fc-fusion would be to utilize a “knob-and-hole” Fc construct. This is a concept that is being explored by Eric Sundberg’s lab at Emory University. The “knob-and-hole” construct requires co-transfection using two different plasmids. One plasmid will contain the protein of interest fused to an Fc protein. The other plasmid will only contain an Fc protein that is designed to dimerize with the Fc protein of the other construct. This will result in the protein of interest being expressed with an Fc dimer that is permanently in the active configuration (**Fig. 2.14**). If this construct works, it may be the most promising way to produce the amounts of asprosin needed to characterize its interaction with PTPRD in the hypothalamus.

Figures

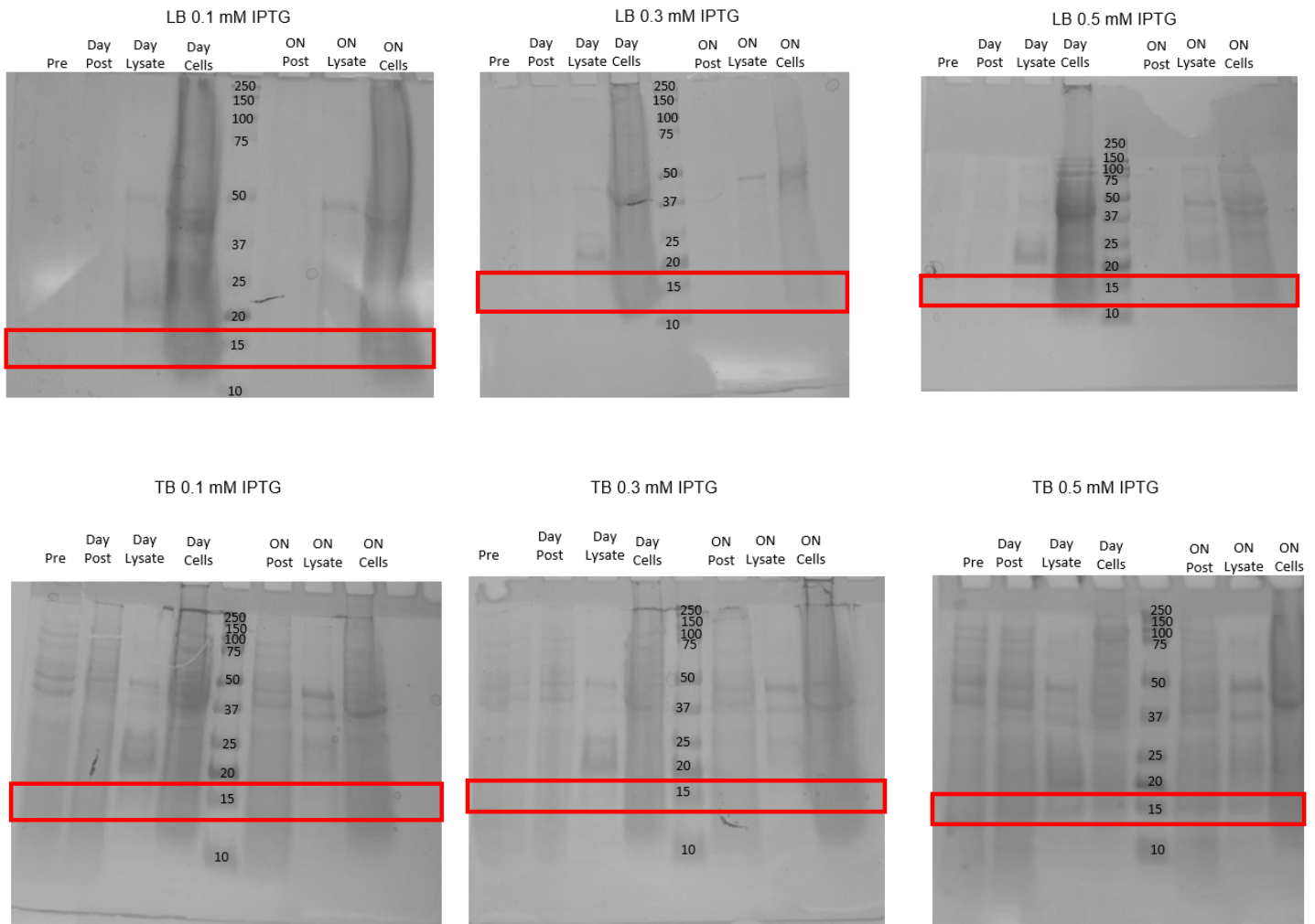


Figure 2.1: *Asprosin in pET-28a(+)* test expressions. Small scale cultures to test for optimal expression conditions for asprosin. Conditions include induction with different concentrations of IPTG, length of growth time, and growth media. For each condition samples were collected pre induction (pre), post induction (post), and from both the cells and the lysate. The red boxes indicated where we would expect to see bacterially expressed asprosin (~17 kDa). There was no indication of asprosin expression from these conditions.

Time (Hrs.)	Tris pH 7.4 (mM)	EDTA (mM)	Urea (M)	Arginine
12	100	5	7	n/a
6	100	5	6	n/a
6	100	5	5	n/a
6	100	5	4	n/a
6	100	5	3	1%
6	100	5	2	1%
6	100	5	1	1%
12	100	5	0	n/a
6	100	5	0	n/a

Table 2.1: Dialysis conditions for stepwise refold of asprosin from inclusion bodies. Buffer components and time courses for each step of dialysis to refold asprosin from denatured inclusion bodies. Dialysis was carried out at room temperature over the specified time courses. Arginine was included in conditions with lower urea concentrations to stabilize protein and prevent aggregation.

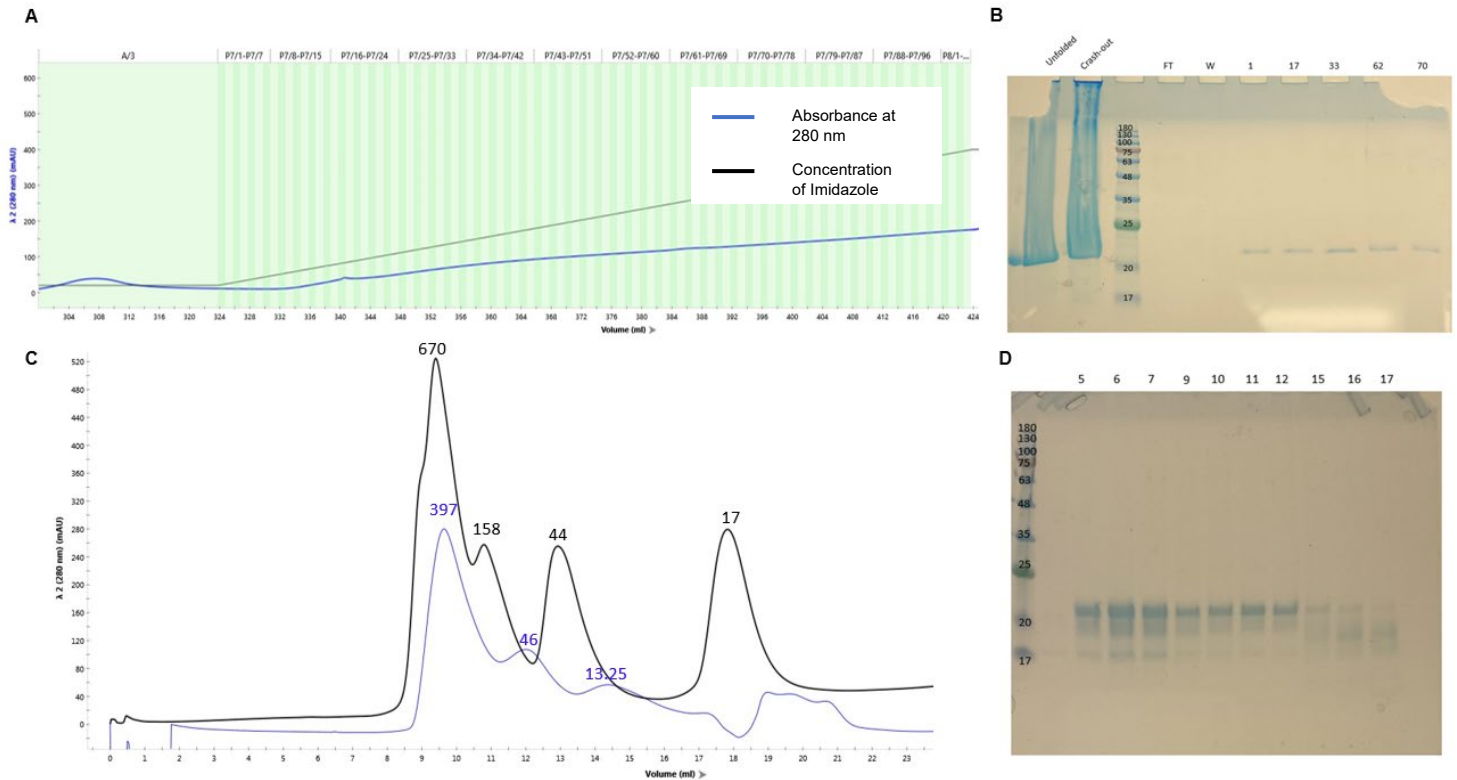


Figure 2.2: *Asprosin* inclusion body stepwise refold. A) Chromatogram from nickel affinity purification of refolded inclusion body product. The protein peak expands throughout the entire chromatogram. B) Fractions collected from the nickel affinity chromatogram, showing pure protein of the expected size (~17 kDa) in every fraction. C) Chromatogram from size-exclusion chromatography. The peaks in black represent the gel filtration standards for the column used. The peaks in blue correspond to the injected protein following refolding and nickel-affinity chromatography. There is no peak corresponding to the expected size for asprosin. D) SDS-PAGE gel containing samples from all three peaks seen in size-exclusion chromatography. There is significant protein degradation observed.

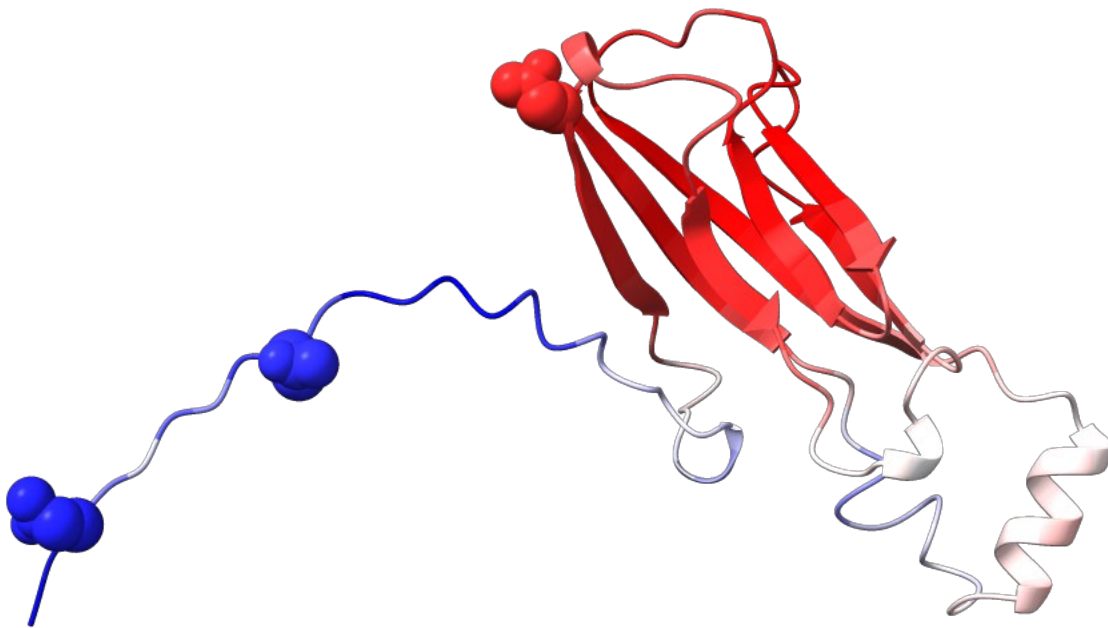


Figure 2.3: Alphafold generated model of asprosin. Predicted 3D structure of asprosin based off of amino acid sequence. The model is colored by confidence of prediction with red being areas of high confidence and blue being areas of low confidence. Predicted N-link glycosylation sites are indicated by spheres.

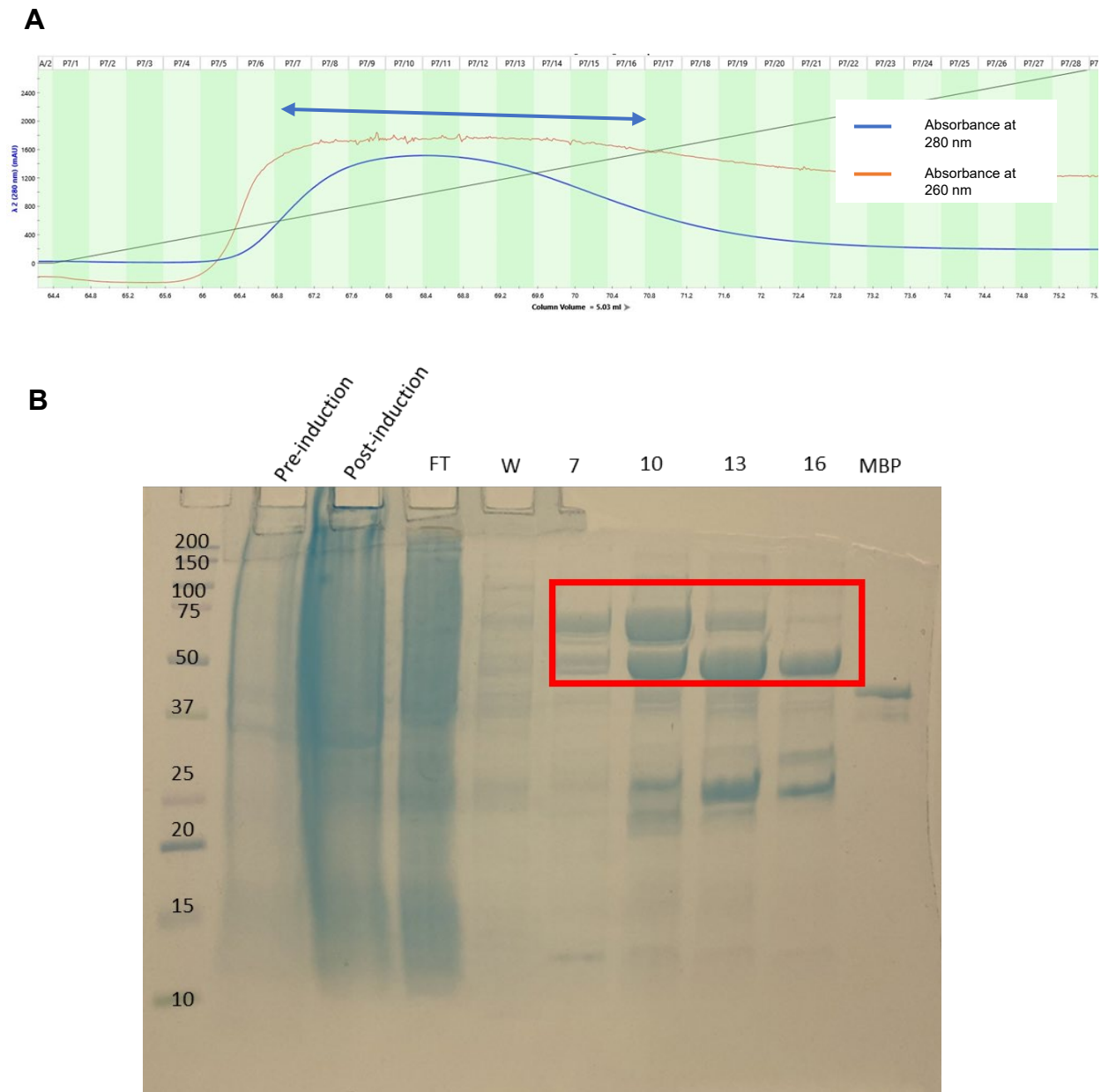


Figure 2.4: Nickel affinity purification of truncated asprosin cleavable MBP construct. A) FPLC Chromatogram of nickel-affinity purification of truncated asprosin cleavable MBP construct. A protein peak was indicated by a peak in absorbance at 280 nm shown in blue. Peak fractions 7-16 were collected as indicated by the arrow. B) Peak fractions were analyzed by SDS-PAGE. Protein of desired size is indicated with the red box. The first half of the peak appears to contain fewer contaminants than the second half. Further purification steps were carried out, separating the peak into each half.

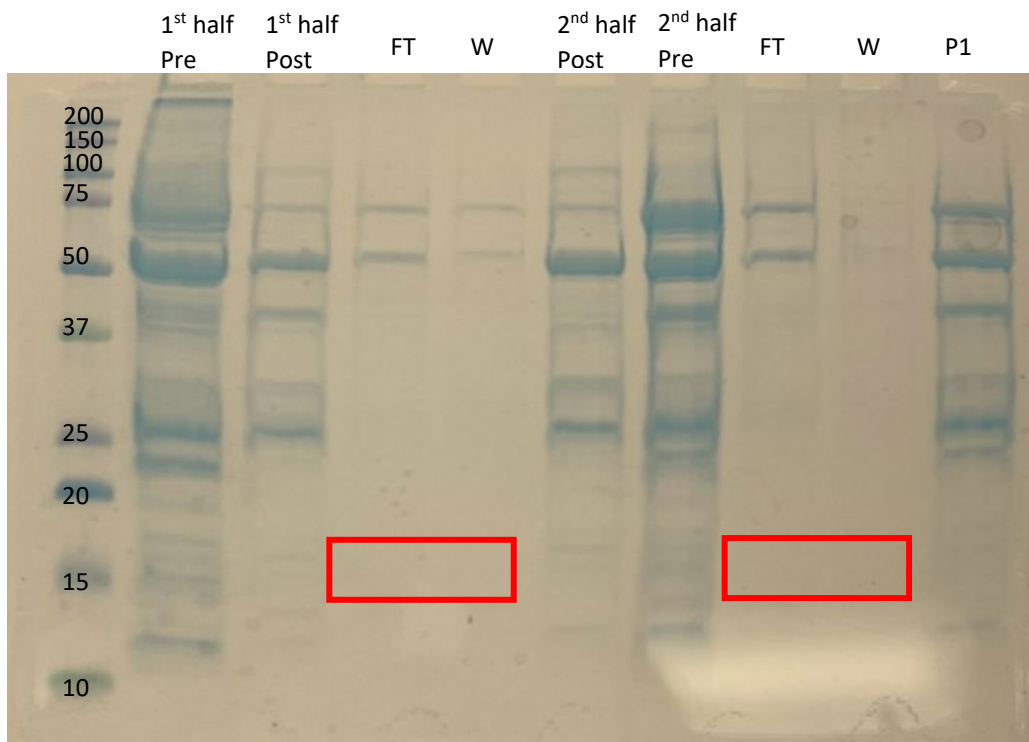


Figure 2.5: Post-TEV cleavage of truncated asprosin cleavable MBP construct. Samples from each half of the protein peak were assessed following TEV cleavage. Red boxes indicate where we would expect cleaved asprosin to run on the gel (~15 kDa). There were small, very faint bands corresponding to protein of the correct size.

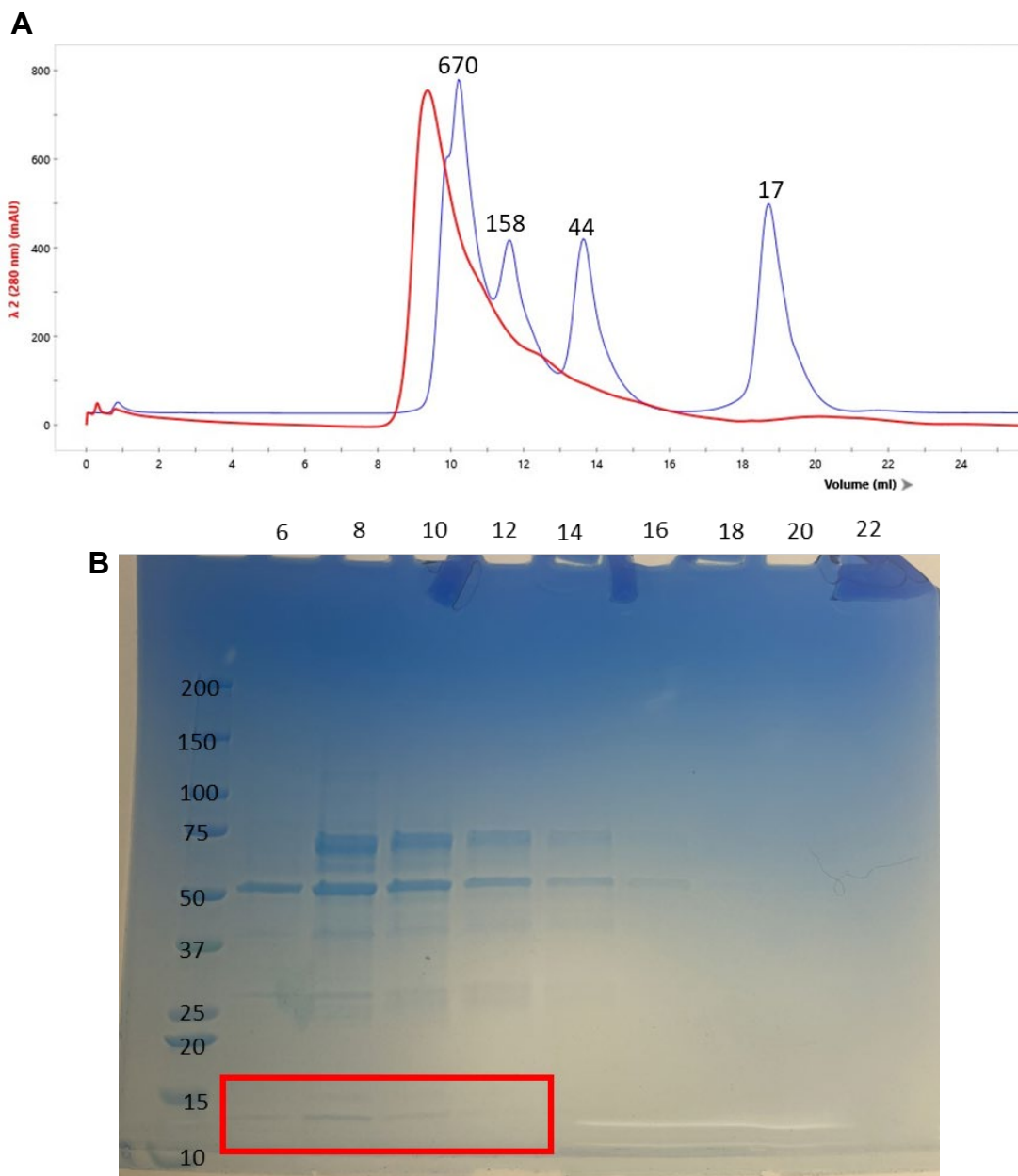


Figure 2.6: SEC of truncated asprosin cleavable MBP post-TEV protease cleavage. A) FPLC chromatogram with size exclusion standards with correlated molecular weights (kDa) shown in blue. Experimental protein peak is shown in red and corresponded to a size greater than 670 kDa (likely aggregation). B) Samples from chromatogram peak analyzed by SDS-PAGE. Protein of desired molecular weight is indicated within the red box. Sample did not contain much of the desired protein and it does not appear to be able to be separated from higher molecular weight proteins.

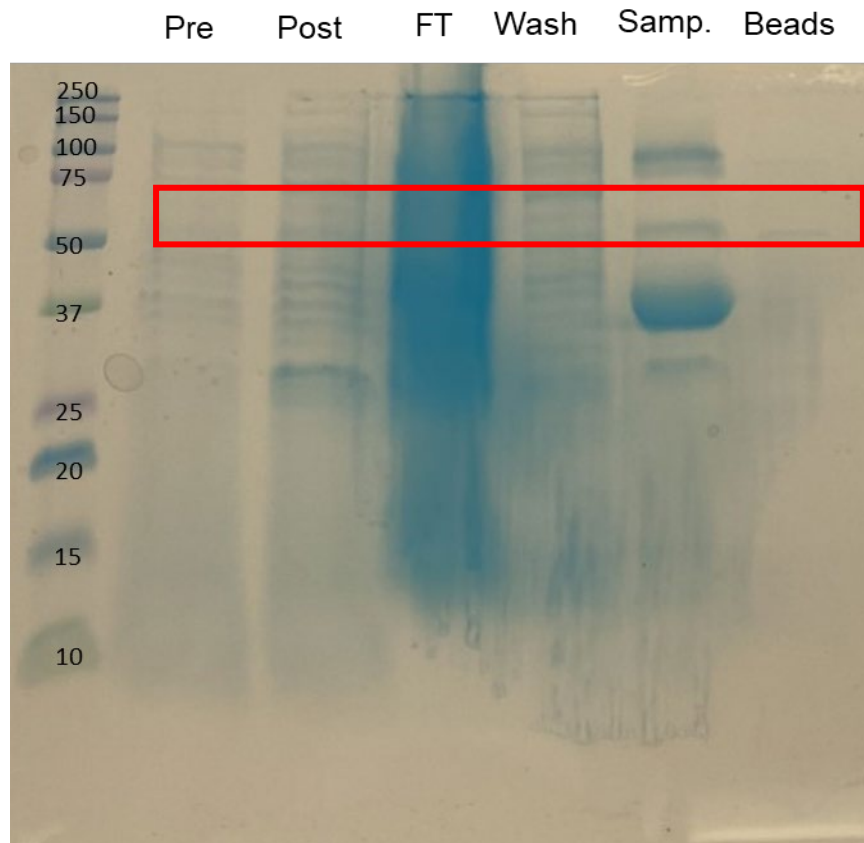
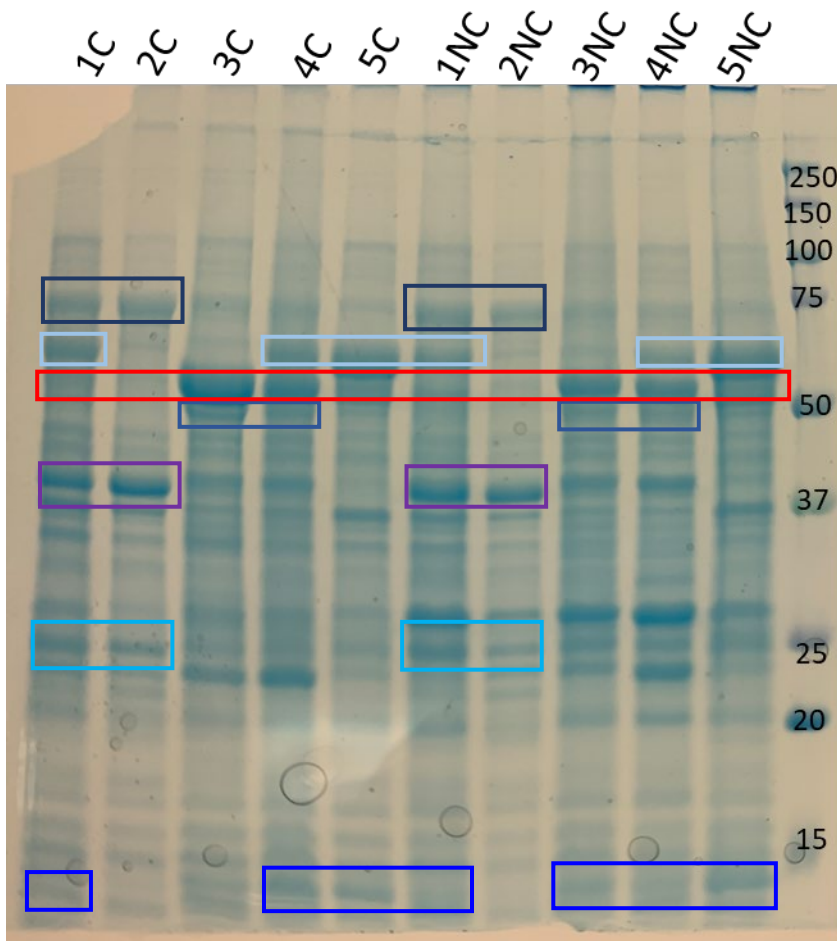


Figure 2.7: Amylose-affinity purification of truncated asprosin rigid MBP construct. Samples of the construct pre-induction with IPTG (pre), post-induction (post), flow-through (FT), wash, the sample eluted with sucrose (sample), and from the amylose beads (beads) were assessed for protein using SDS-PAGE. The red box indicates where we would expect to see purified truncated asprosin rigid MBP, which corresponds to a molecular weight of ~55 kDa. This purification did not yield protein of the expected size.



Chaperone Name	Molecular Weight (kDa)
groES	10 kDa
groEL	58 kDa
grpE	21.8 kDa
Tig	48 kDa
dnaJ	41 kDa
dnaK	70 kDa

Plasmid No.	Plasmid Name	Chaperones	Inducer
1	pF-KJE8	dnaK-dnaJ-grpe groES-groEL	Arabinose & Tetracycline
2	pKJE7	dnaJ-dnaK-grpE	Arabinose
3	pTF16	tig	Arabinose
4	pG-TF2	groES-groEL-tig	Tetracycline
5	pGro7	groES-groEL	Arabinose

Figure 2.8: Test expressions of truncated asprosin MBP-fusion constructs co-expressed with molecular chaperones. Cleavable (C) and non-cleavable (NC) truncated asprosin MBP-fusion constructs were co-expressed with molecular chaperone expression plasmids (1,2,3,4). Molecular chaperones are indicated by coordinated colored boxes. The red box indicates the expected size of the truncated asprosin fusion (~55 kDa). Co-expression with trigger factor (tig) increases expression level of the truncated asprosin MBP fusion.

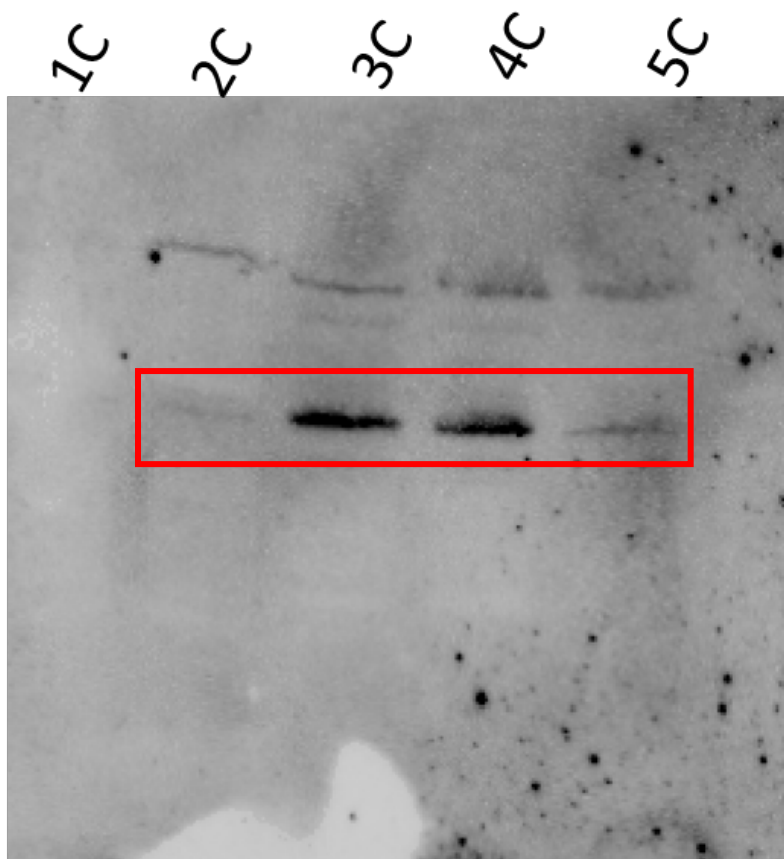


Figure 2.9: Validation of truncated asprosin cleavable MBP expression with molecular chaperones. Identity of truncated asprosin cleavable MBP-fusion was validated using a western blot, blotting for his-tagged protein, using a mouse His-Tag antibody HRP conjugate. His-tagged protein was visualized at the molecular weight expected for the MBP-fusion (~55 kDa).

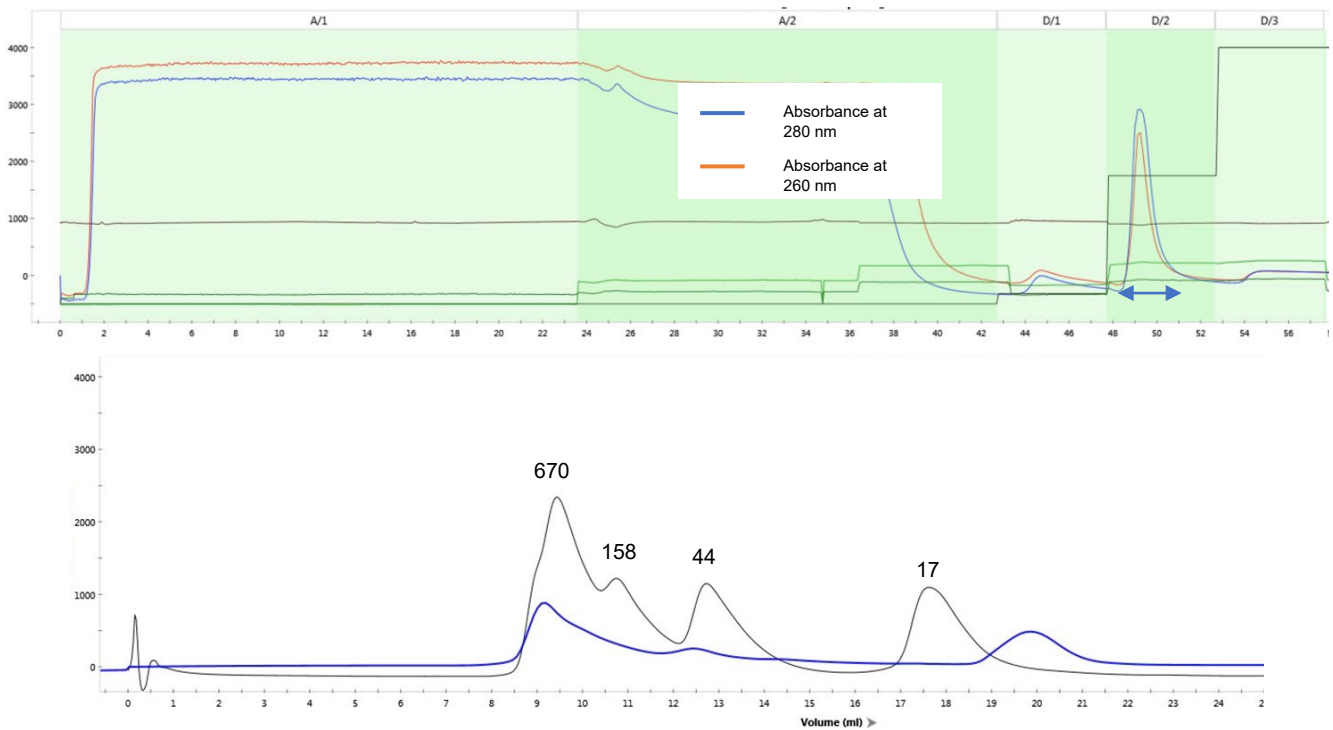


Figure 2.10: Purification of truncated asprosin with cleavable MBP from molecular chaperone co-expression. A) Samples from test-expressions were pooled and purified using nickel-affinity chromatography. Fractions were pooled from the peak on the chromatogram and are indicated with an arrow. B) Peak fractions from nickel-affinity were concentrated and further purified using size exclusion chromatography. Size exclusion standards are indicated in black with their associated molecular weights (kDa). Asprosin-MBP fusion aggregated and was present in the void.

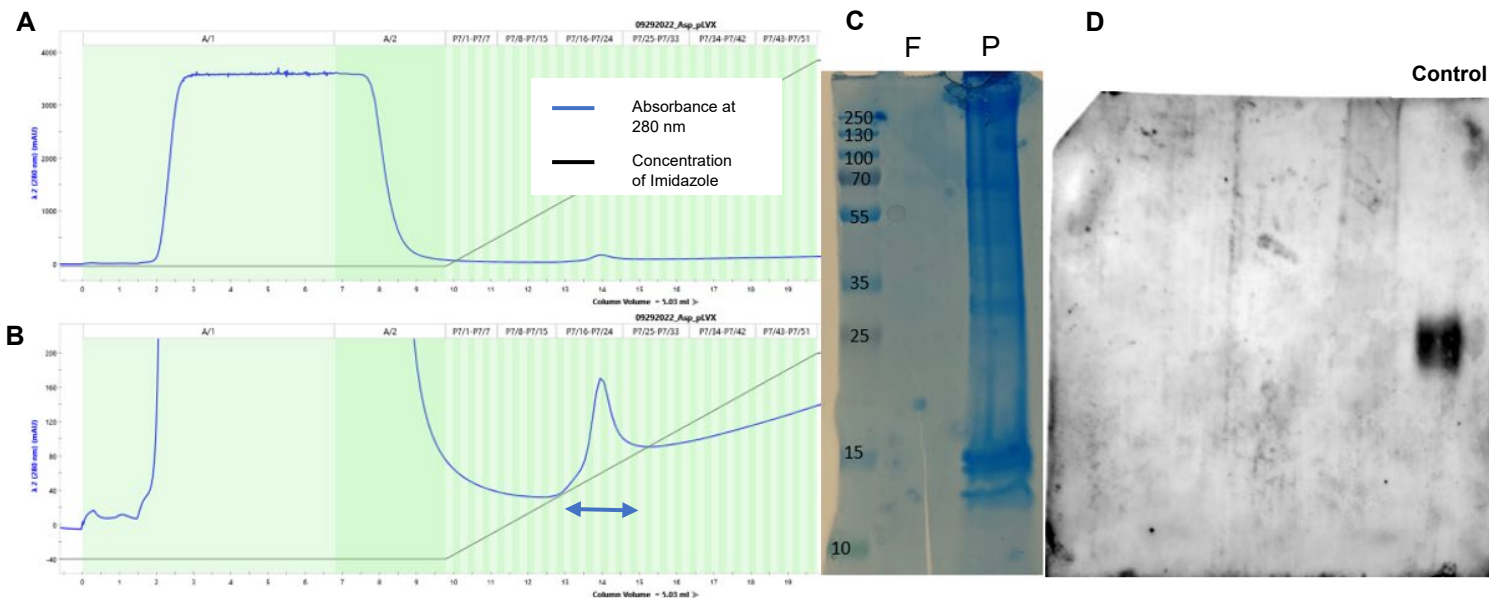


Figure 2.11: Expression of asprosin-pLVX mammalian expression construct. A) Raw chromatogram from nickel affinity chromatography. A small protein peak was present at column volume 14. B) Zoomed in image of nickel-affinity chromatogram. Pooled fractions are indicated by the arrow. C) Pooled fractions (F) were concentrated and assessed for protein purity. Mammalian-expressed asprosin is approximately 30 kDa. No protein of expected size was observed from pooled fractions (F) or from the cell pellet (P). D) Western blot was used to identify if fractions contained asprosin by blotting with mouse anti-asprosin antibody. Purchased asprosin was included as a control. No asprosin was present in pooled fractions.

Name	Sequence (5' → 3')
IL2-FBN-His-For	GATCTATTTCCGGTGATGTACAGGATGCAACTCCT GTCTTGCAATGCACTAAGTCTTGCACTTGTCACGA ACTCGCACCACCACCATCACCAC
IL2-FBN-His-rev	AGGGGCGGGATCCGCTTAATGAAG CAAAACCTGGATTTT

Table 2.2: Primers used for amplification and addition of Gibson arms to asprosin fragment. Red and blue sequences represent Gibson arms that are complementary to those already present on pLVX plasmid. Purple represents a cloned in IL2 leader sequence.

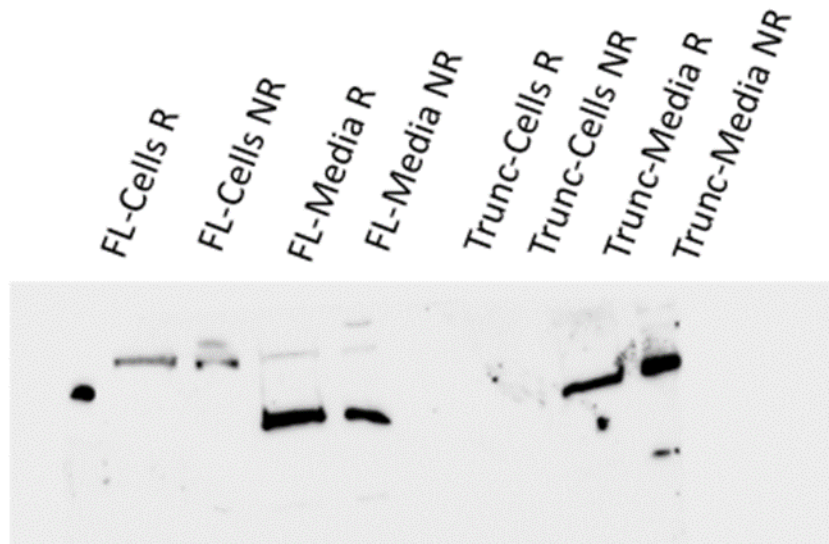


Figure 2.12: Mammalian expression of full-length (FL) asprosin Fc-fusion and Truncated (Trunc) asprosin Fc-fusion. Samples from cells and media of Expi293 cells transfected with asprosin Fc-fusion expression plasmids were collected and analyzed by western blot. Each sample was added to reducing (R) or non-reducing (NR) buffers to assess Fc homodimer formation. Presence of his-tagged protein was visualized using a mouse His-Tag antibody HRP conjugate. His-tagged protein was observed, however, there was no difference in size dependent on reducing or non-reducing conditions. This result indicates lack of an Fc homodimer.

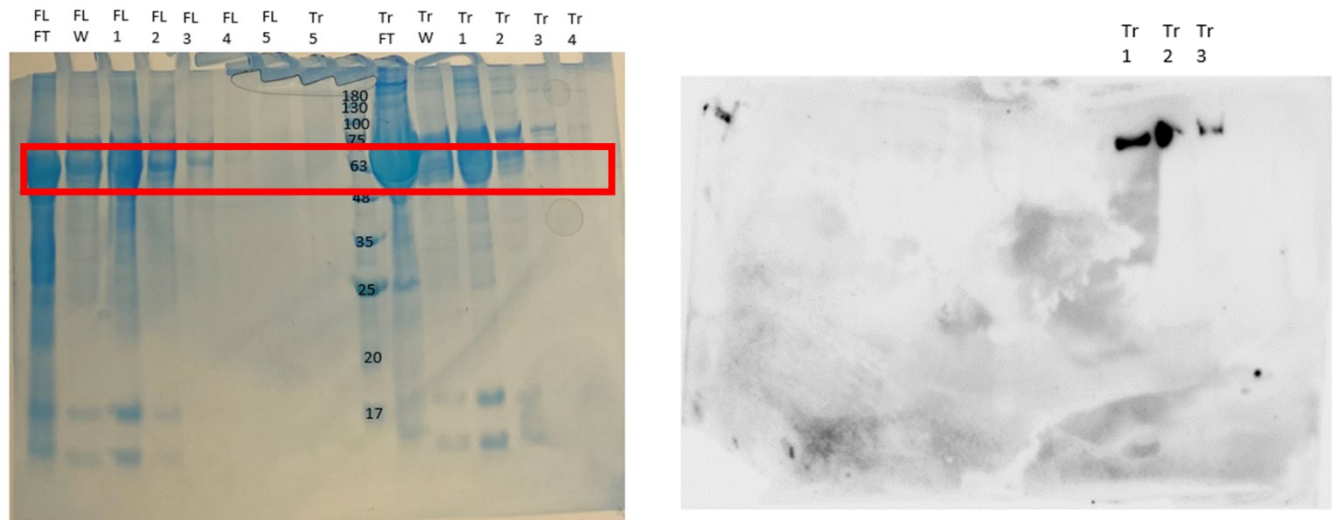


Figure 2.13: Purification of asprosin Fc-fusion constructs using nickel-affinity chromatography. Samples from nickel-affinity purification of full-length asprosin Fc-fusion (FL) and truncated asprosin Fc-fusion (TR) were assessed using SDS-PAGE. The red box indicates the molecular weight we would expect to see the asprosin Fc-fusion (~70 kDa). Fractions were also assessed using western blot blotting for his-tagged protein using a mouse His-Tag antibody HRP conjugate. His-tagged protein was visualized in fractions from the truncated asprosin Fc-fusion construct.

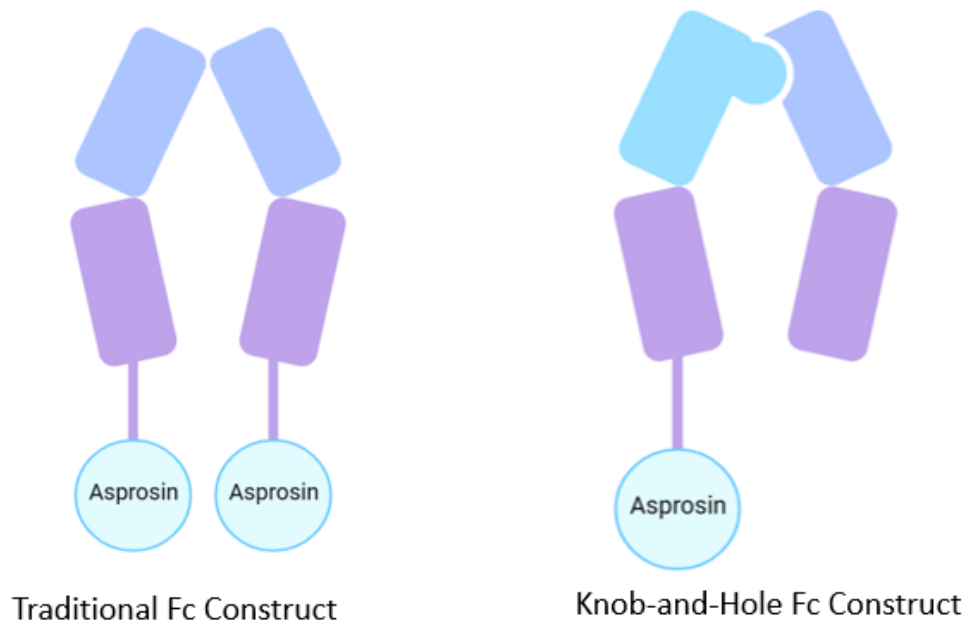


Figure 2.14: Asprosin-Fc fusion representations. This representation highlights the differences between a traditional Fc construct in which asprosin is expressed fused to an Fc immunoglobulin domain, which forms a homodimer and the “knob-and hole” construct in which asprosin is expressed fused to an Fc immunoglobulin domain that is forced into the active state through formation of a heterodimer. This figure was generated in BioRender.

Materials and Methods

Asprosin in pET-28a(+)

A bacterial expression construct of asprosin was designed and cloned into the general bacterial expression backbone, pET-28a(+). The DNA was transformed into BL21 (DE3) E.coli cells for protein expression as His tagged protein. Following transformation, one colony for each protein was picked and added to 20 mL of LB-Amp. These small-scale growths were shaken overnight at 37 °C. The next morning, the overnight cultures were inoculated into separate 1 L cultures of LB-Amp. These large-scale cultures were grown, shaking at 37 °C until they reached an OD600 of 0.6. The cultures were then induced with 0.5 mM IPTG. The cultures continued to grow at 16 °C overnight, while shaking. The following day, the bacteria were centrifugated at 4,500 x g at 4 °C for 30 minutes. Pellets were resuspended in buffer containing 50 mM tris pH 7.4, 500 mM NaCl, and supplemented with PMSF, lysozyme, and DNase. The resuspension was stirred at 4 °C for 30 minutes. Lysis was carried out by sonication on ice. Cellular debris was removed using centrifugation at 16000 x g for one hour at 4 °C. Lysate was purified by nickel affinity chromatography using an FPLC (BioRad).

Refolding asprosin from inclusion bodies

A bacterial expression construct of asprosin was designed and cloned into the general bacterial expression backbone, pET-28a(+). The DNA was transformed into BL21 (DE3) E.coli cells for protein expression as His tagged protein. Following transformation, one colony for each protein was picked and added to 20 mL of LB-Amp. These small-scale growths were shaken overnight at 37 °C. The next morning, the overnight cultures were inoculated into separate 1 L cultures of LB-Amp. These large-scale cultures were grown, shaking at 37 °C until they reached an OD600 of 0.6. The cultures were then

induced with 0.5 mM IPTG. The cultures continued to grow at 37 °C for four hours . After four hours, the bacteria were centrifugated at 4,500 x g at 4 °C for 30 minutes. The pellets were frozen overnight. The next day pellets were thawed and resuspended in buffer containing 50 mM tris pH 7.4, 0.005% triton, 500 mM NaCl, and supplemented with PMSF, lysozyme, and DNase. The resuspension was stirred at 4 °C for 30 minutes. Lysis was carried out by sonication on ice. Cellular debris was removed using centrifugation at 16000 x g for one hour at 4 °C. Following centrifugation there was presence of large inclusion bodies.

The inclusion bodies were washed with a buffer containing 1 M urea, 2% sodium cholate, 100 mM tris pH 7.4, 5 mM EDTA, and 5 mM DTT. Inclusion bodies were washed three times to remove cellular debris. Washed inclusion bodies were denatured with 8M urea, 50 mM tris pH 7.4, and 1 mM EDTA at room temperature overnight. The following morning, dissolved inclusion bodies were measured for total protein concentration. The total protein concentration was diluted to 1 mg/mL in denaturation buffer and inclusion bodies were transferred to 3000 MWCO dialysis tubing. Dialysis conditions were carried out according to **Table 2.1**. Contents of the dialysis tubing were centrifuged at 16000 xg for 30 minutes to remove protein crash out. Samples were pooled and purified using nickel affinity (HiTrap Excel 5 mL column, Cytiva). Protein was eluted from the column using a gradient of imidazole concentrations ranging from 25 mM to 500mM. Fractions from nickel affinity were collected and concentrated using a 10 kDa MWCO Amicon spin filter. An ENrich 70 SEC column (Bio-Rad) was equilibrated in TBS. One mL was injected onto the column followed by a 2 mL wash. Peak fractions were collected and assessed using SDS-PAGE.

Mammalian Expression

Expi293 cells (ThermoFisher Scientific) were thawed and expanded according to manufacturer instructions. Cells were grown to 80% confluency and passaged three times prior to transfection. Cells were grown to a final concentration of 5.6 million cells/mL and then diluted in a 125 mL flask to 3.0 million cells/mL. A complex of plasmid DNA and ExpiFectamine transfection reagent was made and incubated at room temperature for 15 minutes. Following incubation, the transfection complex was added to the 125 mL flask dropwise. Cells were incubated at 37 °C with a humidified atmosphere of 8% CO₂. Twenty-four hours after transfection, transfection enhancers were added to the cells and cells continued to grow at 37 °C shaking at 125 rpm.

Three days post-transfection cell-mass was collected by centrifugation at 500 x g for 10 minutes. Media was collected and filtered using a 0.45 µm sterile syringe filter. Protein was purified from filtered media with a HisTrap Excel 5mL EDTA resistant column (Cytiva) using FPLC (BioRad). Samples were collected and assessed using SDS-PAGE and western blot. A mouse His-Tag antibody HRP conjugate (Novagen) was used to identify presence of his-tagged protein.

References

1. Romere C, Duerrschmid C, Bournat J, Constable P, Jain M, Xia F, Saha PK, Del Solar M, Zhu B, York B, Sarkar P, Rendon DA, Gaber MW, LeMaire SA, Coselli JS, Milewicz DM, Sutton VR, Butte NF, Moore DD, Chopra AR. Asprosin, a Fasting-Induced Glucogenic Protein Hormone. *Cell*. 2016;165(3):566-79. Epub 2016/04/19. doi: 10.1016/j.cell.2016.02.063. PubMed PMID: 27087445; PMCID: PMC4852710.
2. Behrens OK, Bromer WW. Biochemistry of the protein hormones. *Annu Rev Biochem*. 1958;27(3):57-100. Epub 1958/01/01. doi: 10.1146/annurev.bi.27.070158.000421. PubMed PMID: 13571929.
3. Muthu ML, Tiedemann K, Fradette J, Komarova S, Reinhardt DP. Fibrillin-1 regulates white adipose tissue development, homeostasis, and function. *Matrix Biol*. 2022;110:106-28. Epub 2022/05/10. doi: 10.1016/j.matbio.2022.05.002. PubMed PMID: 35533973.
4. Mishra I, Xie WR, Bournat JC, He Y, Wang C, Silva ES, Liu H, Ku Z, Chen Y, Erokwu BO, Jia P, Zhao Z, An Z, Flask CA, He Y, Xu Y, Chopra AR. Protein tyrosine phosphatase receptor δ serves as the orexigenic asprosin receptor. *Cell Metab*. 2022;34(4):549-63.e8. Epub 2022/03/18. doi: 10.1016/j.cmet.2022.02.012. PubMed PMID: 35298903; PMCID: PMC8986618.
5. Wei X, Ao Q, Meng L, Xu Y, Lu C, Tang S, Wang X, Li X. [Expression, purification and functional assessment of asprosin inclusion body]. *Nan Fang Yi Ke Da Xue Xue Bao*. 2020;40(1):67-72. Epub 2020/05/08. doi: 10.12122/j.issn.1673-4254.2020.01.11. PubMed PMID: 32376560; PMCID: PMC7040760.
6. Jumper J, Evans R, Pritzel A, Green T, Figurnov M, Ronneberger O, Tunyasuvunakool K, Bates R, Žídek A, Potapenko A, Bridgland A, Meyer C, Kohl SAA,

Ballard AJ, Cowie A, Romera-Paredes B, Nikolov S, Jain R, Adler J, Back T, Petersen S, Reiman D, Clancy E, Zielinski M, Steinegger M, Pacholska M, Berghammer T, Bodenstein S, Silver D, Vinyals O, Senior AW, Kavukcuoglu K, Kohli P, Hassabis D. Highly accurate protein structure prediction with AlphaFold. *Nature*. 2021;596(7873):583-9. doi: 10.1038/s41586-021-03819-2.

7. Ellis RJ. The molecular chaperone concept. *Semin Cell Biol*. 1990;1(1):1-9. Epub 1990/02/01. PubMed PMID: 1983265.

8. Thomas JG, Ayling A, Baneyx F. Molecular chaperones, folding catalysts, and the recovery of active recombinant proteins from *E. coli*. To fold or to refold. *Appl Biochem Biotechnol*. 1997;66(3):197-238. Epub 1997/06/01. doi: 10.1007/bf02785589. PubMed PMID: 9276922.

9. Czajkowsky DM, Hu J, Shao Z, Pleass RJ. Fc-fusion proteins: new developments and future perspectives. *EMBO Mol Med*. 2012;4(10):1015-28. Epub 2012/07/28. doi: 10.1002/emmm.201201379. PubMed PMID: 22837174; PMCID: PMC3491832.

10. Farrington GK, Caram-Salas N, Haqqani AS, Brunette E, Eldredge J, Pepinsky B, Antognetti G, Baumann E, Ding W, Garber E, Jiang S, Delaney C, Boileau E, Sisk WP, Stanimirovic DB. A novel platform for engineering blood-brain barrier-crossing bispecific biologics. *The FASEB Journal*. 2014;28(11):4764-78. doi: <https://doi.org/10.1096/fj.14-253369>.

Chapter Three: Expression and Purification of Protein Tyrosine Phosphatase Receptor Type D (PTPRD)

Introduction

Recent studies have identified protein tyrosine phosphatase receptor type D (PTPRD) as the receptor that interacts in the hypothalamus with asprosin (1). PTPRD is a member of the protein tyrosine phosphatase (PTP) family proteins, which function in an array of cellular processes, such as cell growth, differentiation, and oncogenic transformation. PTPRD has been a receptor of interest for treatment of cancer due to its role as a tumor suppressor (2). Characterization of PTPRD as a tumor suppressor has revealed that PTPRD has an important role in regulating the phosphorylation status of STAT3 (3), which, as stated previously, also plays an important role in appetite stimulation (4).

Structurally, PTPRD contains an extracellular domain composed of three Ig-like (IgG) domains followed by eight fibronectin type-III-like domains (Fn), a single transmembrane region, and two tandem intracytoplasmic catalytic domains, referred to as D1 and D2 (5). PTPRD belongs to a subset of PTPs known as type-IIa receptor PTPs, which share a common general structure. Type IIa receptor PTPs contain splicing sites within their IgG domains that confer binding specificity. These splicing sites generate short-peptide inserts, referred to as mini-exon peptides (Me) (6). Type IIa receptor PTPs all contain two splicing sites, MeA and MeB (7, 8). MeB shares a common amino acid sequence among Type IIa receptor PTPs, however there are several isoforms of MeA that vary in length (9). PTPRD is unique in that it contains an MeA peptide that has nine amino acid residues (9), which may aid in specific recognition of PTPRD by asprosin and other ligands. Dimerization of receptor PTPs is known to regulate their catalytic function (10).

Crystal structure analysis of 22 different PTPs revealed that PTP dimerization occurs in two different conformations, head-to-toe and wedge conformation (10). Dimerization has been proposed to be the mechanism that de-activates PTPs. Analytical centrifugation (AUC) data has shown that most PTPs exist as monomers in solution. However, RPTP γ , has been shown to dimerize in a concentration-dependent manner (10). While PTPRD was not included in this initial structural study of PTPs, preliminary characterization of PTPRD suggests that it may be similar to RPTP γ and is active in its dimeric state.

The interaction between asprosin and PTPRD has been initially characterized using binding assays, such as bio-layer interferometry (BLI), analytical ultra-centrifugation (AUC), and surface plasmon resonance (SPR) (1). These initial binding assays were performed using the full-length PTPRD extracellular domain. While these assays confirmed that asprosin is interacting with PTPRD with a high affinity (nanomolar affinity), we are interested in determining if the entire extracellular domain is needed for this interaction. We aimed to determine this both structurally and biochemically. For the biochemical assays planned, it was important to purify the domain regions of PTPRD individually. It was predicted that the IgG domains of PTPRD would be the most important component for the interaction with asprosin, as this is the region of the protein that contains the mini-exon peptides, which are suspected to be important in conferring protein binding specificity.

Results

PTPRD Domains

Truncated constructs of the extracellular region of PTPRD were cloned, expressed, and purified to facilitate the proposed domain mapping experiments. One construct contains the three IgG domains and the other contains the eight Fn domains. The PTPRD truncated domain (IgG and Fn) constructs each contain a maltose binding protein (MBP) tag and a his-tag on the N-terminus. Positive clones of each construct were confirmed by sequencing. The final bacterial expression plasmids are represented in **Fig. 3.1**. PTPRD-IgG-MBP and PTPRD-Fn-MBP were expressed in *E. coli* BL21(DE3) and purified by Nickel affinity chromatography. Fractions from the peaks of each elution profile were pooled and further purified using anion exchange chromatography and size exclusion chromatography (**Fig. 3.2 and Fig. 3.3**). The final SDS-PAGE gels indicated that the proteins were sufficiently pure for use in functional studies (**Fig. 3.4**).

Full-Length PTPRD Extracellular Domain

It is desirable to also express and purify the full-length extracellular domain of PTPRD from bacterial cells, which will be used for structural studies. Previous studies with PTPRD have been done using mammalian expressed proteins. PTPRD contains N-linked glycosylation sites within the Fn domains of the protein. It is possible that these sites will cause bacterial expression of the full extracellular region to be difficult.

I cloned, expressed, and purified a construct of the extracellular region of PTPRD. The PTPRD extracellular region was expressed in bacteria with a maltose binding protein (MBP) tag and a his-tag on the N-terminus. The maltose binding protein is able to be cleaved for structural studies, as it was cloned with a TEV protease cleavage site following the protein. PTPRD-FL-MBP was expressed in *E. coli* BL21(DE3) and purified by Nickel

affinity chromatography. Fractions from the peaks of each elution profile were pooled and further purified using anion exchange chromatography and size exclusion chromatography. The final SDS-PAGE gels indicated that the protein was degraded or cleaved during purification. This process was repeated several times with the same result. This may suggest that there is a protease cleavage site or that glycosylation is necessary for protein expression and purification. PTPRD for structural studies will need to be expressed in mammalian cells.

Crystallizable PTPRD

A previous structural study was able to crystallize a partial construct of the extracellular region of PTPRD in complex with its binding partners, interleukin-1 receptor accessory protein (IL-1RAcP) and IL-1RAcP-like-1 (IL1RAPL1) (8). The partial construct used in this paper consisted of all three IgG domains and two of the Fn domains (IgG1-Fn2), expressed in mammalian cells. This construct is crystallizable and seems sufficient for binding, so we hypothesized that maybe this construct could be used for crystallization of PTPRD with asprosin.

I initially began work with crystallizable PTPRD by designing two different constructs. One construct contained crystallizable PTPRD in the vector backbone pcDNA3.1, which is a general mammalian expression vector. I chose to use this vector as this is most similar to the vector that was used in the crystallization paper. I designed a second construct of this protein that contained crystallizable PTPRD in the vector backbone PAH. PAH is a commonly used vector that can be used to establish a stable cell line through adenovirus production. A stable cell line may be utilized in the future if efforts with this construct are successful.

Issues with this construct began in the cloning stage. I amplified both the crystallizable PTPRD insert and vector backbone using PCR. Gibson assembly was used to clone these constructs, so complimentary Gibson arms were appended to both the insert and the vector during PCR. Agarose gel analysis post PCR indicated that amplification of both vectors and inserts were successful. PCR amplification was followed by *dpnI* digestion and PCR cleanup (QIAGEN). Gibson assembly was carried out for each construct, using a vector-only control as a negative control. Following Gibson assembly, the reactions were transformed into *E. coli* DH5 α cells, and plated on agarose plates supplemented with ampicillin. The Gibson reactions appeared successful, as I had many colonies on my reaction plates and no colonies on my negative control. I screened eight colonies from each experimental plate and sent them for sequencing. Sequencing revealed that each of the constructs did not contain the crystallizable PTPRD insert, but instead contained the original insert that was in each of the vector backbones. It is likely that *dpnI* digestion was incomplete. New cloning strategies will need to be explored to generate these constructs.

Discussion

Expression and purification of individual PTPRD extracellular domains from *E. coli* was a success. However, the same expression and purification strategy cannot be applied to the full-length extracellular domain of PTPRD. Bacterial expression of the full extracellular domain of PTPRD resulted in a truncated, degraded protein product that will not be sufficient for biochemical or structural studies. Expression and purification of this protein will need to be achieved through other expression strategies. It is possible that this protein could be properly expressed in insect or mammalian cell lines.

The crystallizable PTPRD construct is still a viable and exciting option for PTPRD production for structural studies. Success of this method relies on troubleshooting with cloning to ensure that the correct insert is in the correct vector backbone. It is possible that proper digestion of parent DNA with *dpn1* was not achieved. To remedy this issue, fresh *dpn1* should be used and digestion should be carried out for a longer period of time.

Figures

Name	Sequence (5' → 3')
MBP-TEV for	GAT CCG GCT GCT AAC AAA GCC CGAAAG GAA GCT GAT
MBP-rev	GGA TTG GAA GTA CAG GTT CTC GGT ACC TGG GAT ATC
PTPRD IgG MBP for	ACC GAG AAC CTG TAC TTC CAA TCC AGA TTC ACC AGAACA CCC GTG
PTPRD IgG MBP rev	GGA TTT GTT AGC AGC CGG ATC CTA CTT CTC AAA TTG AGG GTG
PTPRD Fn MBP for	ACC GAG AAC CTG TAC TTC CAA TCC GGC ACC CCT GTA GTG ACC
PTPRD Fn MBP rev	GGA TTT GTT AGC AGC CGG ATC CTA CTT CTC AAA TTG GGG TGG
PTPRD Full Length MBP for	ACC GAG AAC CTG TAC TTC CAA TCC ATG TAC AGG ATG CAA CTC CTG TCT
PTPRD Full Length MBP rev	GGA TTT GTT AGC AGC CGG ATC CTA TTC TTC TTC ATC CGT GAT

Table 3.1: Primers used for generation of PTPRD Expression Plasmids. The colored sequences highlight the regions of DNA overlap required for Gibson Assembly.

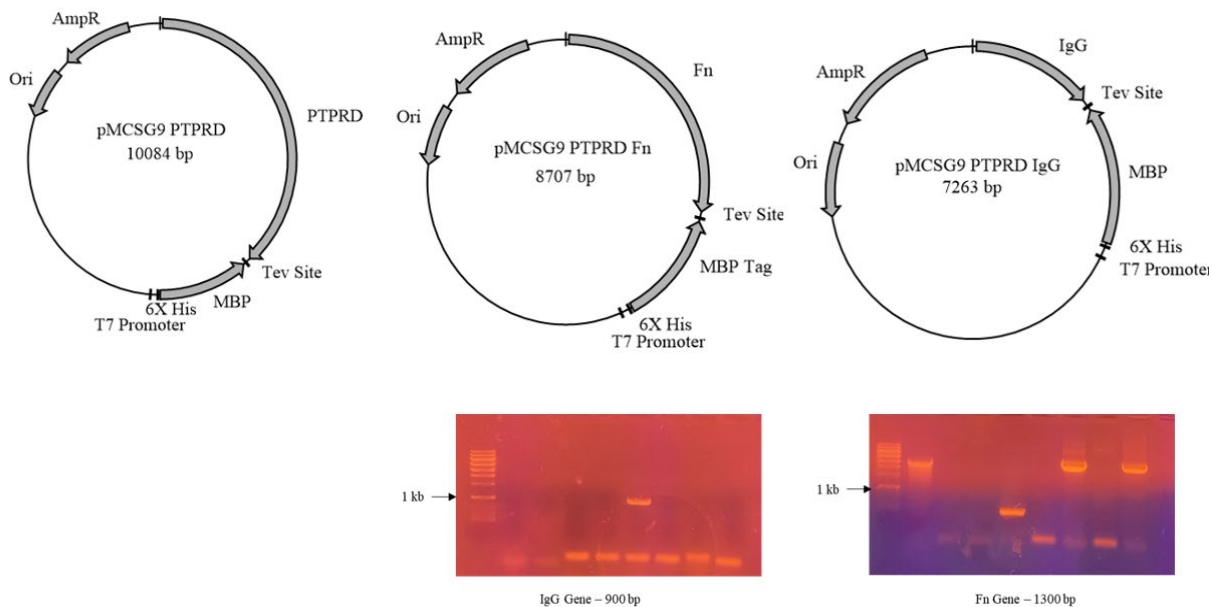


Figure 3.1: PTPRD Truncation Expression Plasmids. All of the expression plasmids contain a gene encoding an MBP tag and a 6X His tag. Each of the expression plasmids expressed resistance to Ampicillin. The agarose gels indicate positive clones for the IgG domain and Fn domain.

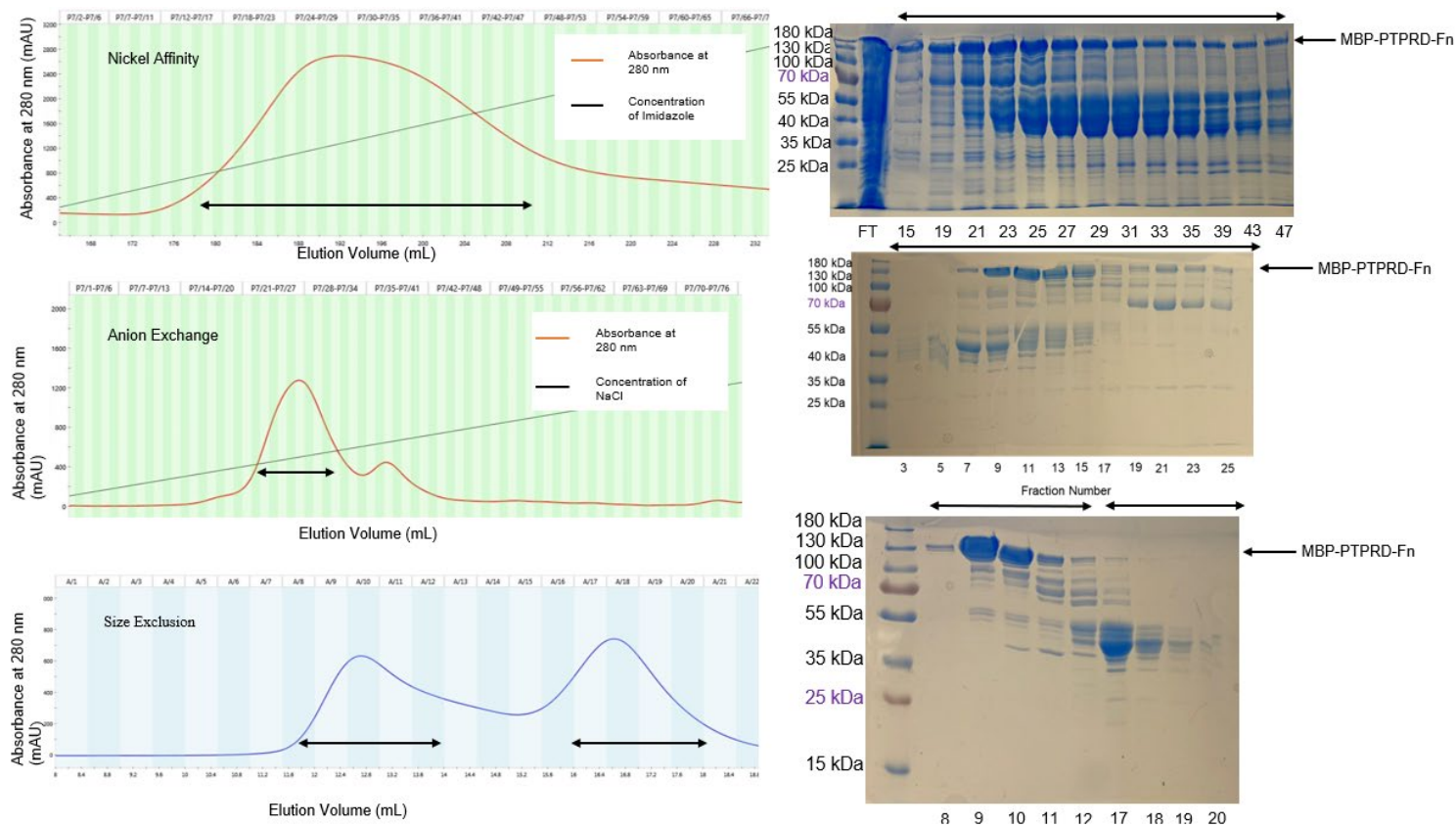


Figure 3.2: Purification scheme for PTPRD-Fn. The elution profiles and corresponding SDS-PAGE gels for each step of purification for PTPRD-Fn. Arrows indicate the fractions selected for SDS-PAGE analysis. The final protein is pure enough for biochemical assays.

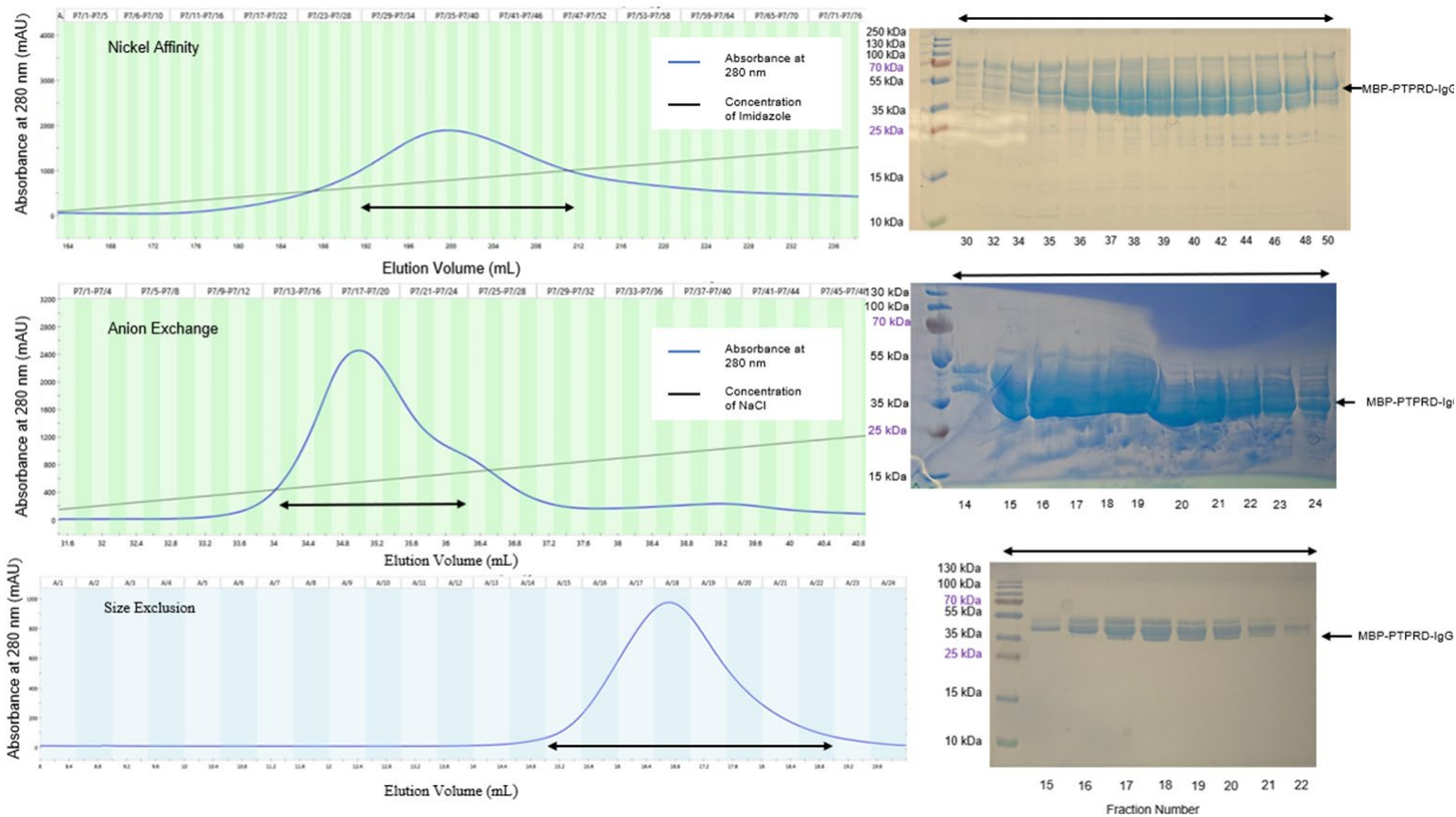


Figure 3.3: Purification Scheme of PTPRD-IgG. Elution profiles and corresponding SDS-PAGE gels for each step of purification for the PTPRD-IgG domain. Arrows indicate peak fractions selected for SDS-PAGE analysis. The final protein is mostly pure, however the doublet band visible in the SDS-PAGE gel may indicate protein degradation product.

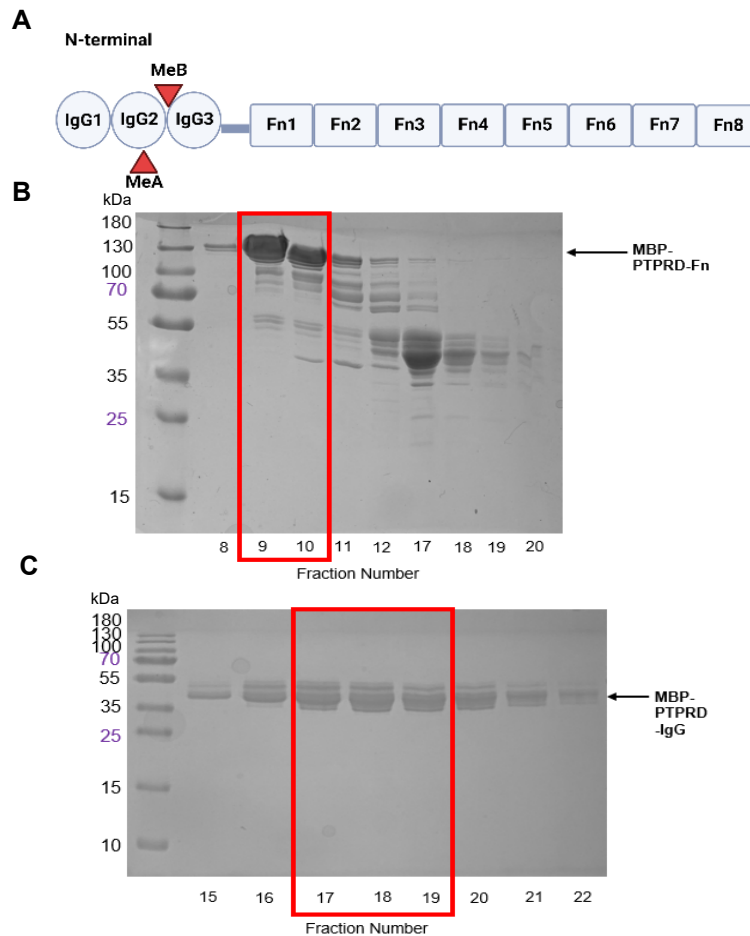


Figure 3.4: Purity of PTPRD domains following size-exclusion chromatography. A) Schematic representation of the PTPRD extracellular domain with MeA and MeB sites indicated with red arrows. B) Purified 6XHis-MBP tagged PTPRD-FN. The expected size of PTPRD- Fn is 110 kDa. C) Purified 6XHis-MBP tagged PTPRD-IgG. The expected size of PTPRD-IgG is 50 kDa. Collected fractions are indicated by red boxes. Together, these data verify that purified PTPRD truncations are of the expected size and purity to be used in functional in vitro studies.

Name	Sequence (5' → 3')
PTPRD_ig1-fn2_pcDNA3.1_FOR	AAGCTGGCTAGCGCCACCGCCACCATG TACAGGATGCAAC
PTPRD_ig1-fn2_pcdna3.1_REV	CTCGGTACCTCAAGACTCAGGTTCTGCT TTGAAGTTTAGTG
pcDNA3.1_cry_PTPRD_FOR	TCAAAGCAGAACCTGAGTCTTGAGGTAC CGAGCTCGGATC
pcDNA3.1_cry_PTPRD_REV	GAGTTGCATCCTGTACATGGTGGCGGTG GCGCTAGCCAGC
PTPRD_ig1-fn2_PAH_FOR	GAATTATCGCTCGAGCTATTAGCCACCAT GTACAGGATGCAAC
PTPRD_ig1-Fn2_PAH_REV	CATCACCACTCAAGACTCAGGTTCTGCT TTGAAGTTTAGTG
PAH_PTPRD_cry_FOR	CAAAGCAGAACCTGAGTCTTGAGTGGT GATGGTGGTGGTG
PAH_cry_PTPRD_REV	GTACATGGTGGCTAATAGCTCGAGCGAT AATCACTCCTCAG

Table 3.2: Primers used for generation of crystallizable PTPRD construct. The colored sequences highlight the regions of DNA overlap required for Gibson Assembly.

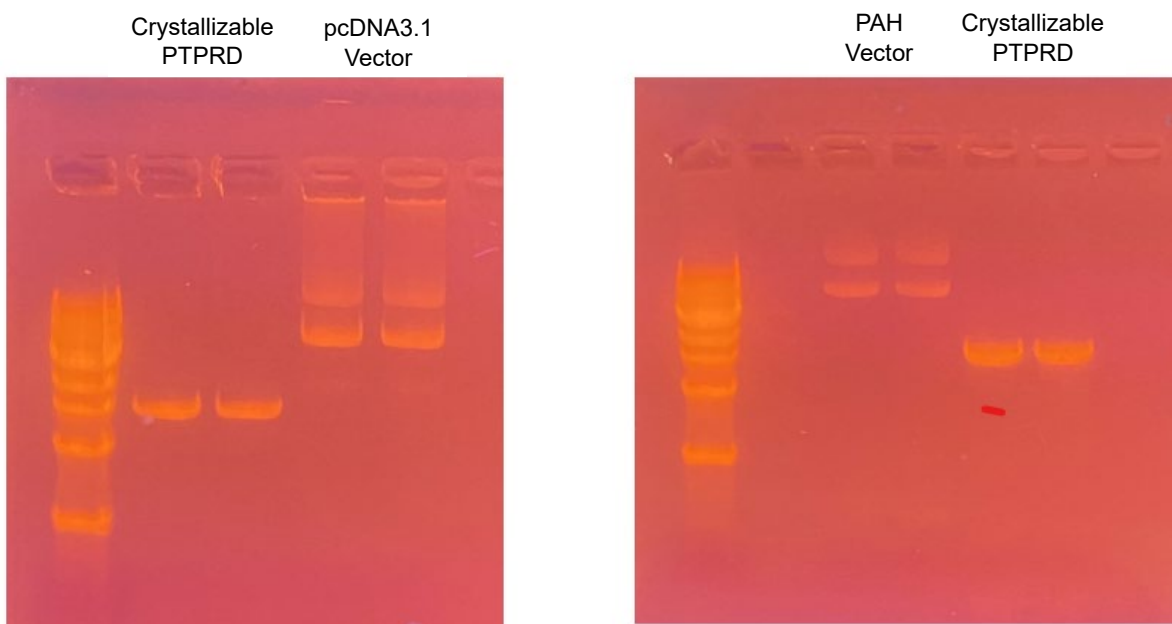


Figure 3.5: PCR amplification of crystallizable PTPRD. PCR was used to amplify the crystallizable PTPRD (Ig1-Fn2) domains and the vector backbones of pcDNA 3.1 and PAH. Overlapping Gibson arms were added to each fragment for use in Gibson assembly.

Materials and Methods

Cloning

The PTPRD truncated domains (IgG and Fn), as well as the full-length extracellular region were received in the mammalian expression plasmids, pcDNA3.1. Each of the constructs express the gene of interest with a 6X His tag on the N-terminus. A bacterial expression plasmid was generated using Gibson Assembly. The primers utilized for addition of Gibson arms were designed and are included in **Table 3.1**. The fragments for the coding region of each of the domains of the PTPRD receptor, the full length PTPRD receptor, as well as the backbone for the plasmid, pMCSG9, were amplified and overlapping DNA fragments were added to the ends of each fragment using PCR. PCR was carried out under the following conditions: Denaturation for 30s at 98 °C, followed by 30 cycles of 30s at 98 °C, 30s at 58 °C, and 40s per kb at 72 °C, followed by an elongation of 10 min at 72 °C. The amplified fragments were verified with visualization on a 1% agarose gel with ethidium bromide ran in 1X Tris Acetate EDTA (TAE) buffer. The amplified fragments that were of the expected size were digested with DpnI restriction enzyme overnight at 37 °C to degrade template DNA plasmid. Following overnight digestion, the amplified fragments were purified using the QIAquick PCR Purification Kit (QIAGEN).

Gibson Assembly was carried out for each of the PTPRD truncation constructs according to the manufacturer's instructions (New England BioLabs). Eight colonies from each Gibson Assembly reaction were inoculated into 6 mL of LB supplemented with ampicillin. DNA extraction was performed using QIAprep Spin Miniprep Kit (QIAGEN) according to the manufacturer's instructions. Positive clones of each construct were confirmed by sequencing. The final bacterial expression plasmids are represented in **Figure 3.1**.

The same cloning workflow was used for generation of crystallizable PTPRD constructs. Primers used for addition of Gibson arms are included in **Table 3.2**.

Protein Expression and Purification

DNA of each designed construct was transformed into BL21 (DE3) *E. coli* cells for protein expression as His-MBP tagged protein. Following transformation, one colony for each protein was picked and added to 20 mL of LB supplemented with ampicillin. These small-scale growths were shaken overnight at 37 °C. The next morning, the overnight cultures were inoculated into separate 1 L cultures of LB supplemented with ampicillin. These large-scale cultures were grown, shaking at 37 °C until they reached an OD₆₀₀ of 0.6. The cultures were then induced with 0.5 mM isopropylthio-β-D-galactoside (IPTG). The cultures continued to grow at 16 °C overnight, while shaking. The following day, the bacteria were centrifugated at 4,500 x g at 4 °C for 30 minutes. The pellets were saved at -20 °C until ready for purification.

The pellets for each protein were resuspended in lysis buffer (20 mM Tris pH 7.5, 150 mM NaCl, 5% glycerol, 0.5 mM tris(2-carboxyethyl)phosphine (TCEP), and 20 mM imidazole). The resuspended pellet was subjected to sonication for 10 minutes with pulses of 1 second on and 1 second off. Following sonication, samples were centrifugated at a speed of 33,000 x g for 45 minutes at 4 °C. The supernatant was collected and purified by affinity chromatography using fast protein liquid chromatography (FPLC). A HisTrap HP 5 mL column (Sigma-Aldrich) was equilibrated with wash buffer (20 mM Tris pH 7.5, 150 mM NaCl, 5% glycerol, and 0.5 mM TCEP). The sample was added to the column and non-specific binding proteins were eluted with wash buffer and 25 mM imidazole. A gradient ranging from 25 mM to 500 mM imidazole was used to find an

optimal imidazole concentration for elution and 1 mL fractions were collected. The purity of each fraction within the elution peak were analyzed by SDS-PAGE. Samples from fractions within elution peak were loaded onto a 12% polyacrylamide gel. Following electrophoresis, the proteins were visualized by staining with Coomassie brilliant blue. The SDS-PAGE gels of PTPRD-Fn and PTPRD-IgG fractions contained bands correlating to the size of the protein with the MBP tag (~110 kDa and 60 kDa respectively). The samples of PTPRD-Fn and PTPRD-IgG still contained contaminants of other non-specific proteins at this step (**Fig. 3.2 and Fig. 3.3**).

The proteins were further purified using anion exchange chromatography, which separates proteins based on their charge. The peak protein fractions were collected for each protein and each protein was diluted to 50 mM NaCl with salt-free buffer (20 mM Tris pH 7.5, 5% glycerol, and 0.5 mM TCEP). A HiTrap Q HP 5 mL column (Sigma-Aldrich) was equilibrated with salt-free buffer. The sample was added to the column and non-specific binding proteins were eluted with salt free buffer and 50 mM NaCl. The protein of interest was eluted from the column with a gradient ranging from 50 mM elution buffer to 1 M NaCl. Fractions were collected and analyzed by SDS-PAGE. Following anion-exchange chromatography, the purity of each protein was improved significantly (**Fig. 3.2 and Fig. 3.3**).

The final step of purification was size exclusion chromatography. The PTPRD-Fn protein was concentrated to 1.5 mL of 7.6 mg/mL protein. A Superdex Increase 200 10/300 GL column (Sigma-Aldrich) was equilibrated with size exclusion buffer (20mM HEPES pH 7.5, 150 mM NaCl, and 0.5 mM TCEP). Following equilibration, 1.0 mL of PTPRD-Fn sample was injected onto the column. The protein was eluted from the column

with 35.0 mL of size exclusion buffer. Two peaks eluted from the column. The peak corresponding to purified PTPRD-Fn was determined using SDS-PAGE (**Fig. 3.2**). The peak fractions were flash frozen and kept at -80 °C for future use in biochemical assays. The PTPRD-IgG domain was concentrated to 1.5 mL of 6.5 mg/mL protein. The same size exclusion protocol described above was used for PTPRD-IgG. SDS-PAGE of peak fractions of PTPRD-IgG showed pure protein, however there was a doublet band observed at the expected weight (**Fig. 3.3**). Peak fractions were flash frozen and kept at -80 °C for future use in biochemical assays.

References

1. Mishra I, Xie WR, Bournat JC, He Y, Wang C, Silva ES, Liu H, Ku Z, Chen Y, Erokwu BO, Jia P, Zhao Z, An Z, Flask CA, He Y, Xu Y, Chopra AR. Protein tyrosine phosphatase receptor δ serves as the orexigenic asprosin receptor. *Cell Metab.* 2022;34(4):549-63.e8. Epub 2022/03/18. doi: 10.1016/j.cmet.2022.02.012. PubMed PMID: 35298903; PMCID: PMC8986618.
2. Veeriah S, Brennan C, Meng S, Singh B, Fagin JA, Solit DB, Paty PB, Rohle D, Vivanco I, Chmielecki J, Pao W, Ladanyi M, Gerald WL, Liao L, Cloughesy TC, Mischel PS, Sander C, Taylor B, Schultz N, Major J, Heguy A, Fang F, Mellinghoff IK, Chan TA. The tyrosine phosphatase PTPRD is a tumor suppressor that is frequently inactivated and mutated in glioblastoma and other human cancers. *Proc Natl Acad Sci U S A.* 2009;106(23):9435-40. Epub 2009/05/30. doi: 10.1073/pnas.0900571106. PubMed PMID: 19478061; PMCID: PMC2687998.
3. Ortiz B, Fabius AW, Wu WH, Pedraza A, Brennan CW, Schultz N, Pitter KL, Bromberg JF, Huse JT, Holland EC, Chan TA. Loss of the tyrosine phosphatase PTPRD leads to aberrant STAT3 activation and promotes gliomagenesis. *Proc Natl Acad Sci U S A.* 2014;111(22):8149-54. Epub 2014/05/21. doi: 10.1073/pnas.1401952111. PubMed PMID: 24843164; PMCID: PMC4050622.
4. Derghal A, Astier J, Sicard F, Couturier C, Landrier JF, Mounien L. Leptin Modulates the Expression of miRNAs-Targeting POMC mRNA by the JAK2-STAT3 and PI3K-Akt Pathways. *J Clin Med.* 2019;8(12). Epub 2019/12/19. doi: 10.3390/jcm8122213. PubMed PMID: 31847355; PMCID: PMC6947463.

5. Kim M, Morales LD, Jang IS, Cho YY, Kim DJ. Protein Tyrosine Phosphatases as Potential Regulators of STAT3 Signaling. *Int J Mol Sci.* 2018;19(9). Epub 2018/09/14. doi: 10.3390/ijms19092708. PubMed PMID: 30208623; PMCID: PMC6164089.
6. Um JW, Kim KH, Park BS, Choi Y, Kim D, Kim CY, Kim SJ, Kim M, Ko JS, Lee SG, Choi G, Nam J, Heo WD, Kim E, Lee JO, Ko J, Kim HM. Structural basis for LAR-RPTP/Slietrk complex-mediated synaptic adhesion. *Nat Commun.* 2014;5:5423. Epub 2014/11/15. doi: 10.1038/ncomms6423. PubMed PMID: 25394468.
7. Yoshida T, Shiroshima T, Lee SJ, Yasumura M, Uemura T, Chen X, Iwakura Y, Mishina M. Interleukin-1 receptor accessory protein organizes neuronal synaptogenesis as a cell adhesion molecule. *J Neurosci.* 2012;32(8):2588-600. Epub 2012/02/24. doi: 10.1523/jneurosci.4637-11.2012. PubMed PMID: 22357843; PMCID: PMC6621890.
8. Yoshida T, Yasumura M, Uemura T, Lee SJ, Ra M, Taguchi R, Iwakura Y, Mishina M. IL-1 receptor accessory protein-like 1 associated with mental retardation and autism mediates synapse formation by trans-synaptic interaction with protein tyrosine phosphatase δ . *J Neurosci.* 2011;31(38):13485-99. Epub 2011/09/24. doi: 10.1523/jneurosci.2136-11.2011. PubMed PMID: 21940441; PMCID: PMC6623287.
9. Yamagata A, Yoshida T, Sato Y, Goto-Ito S, Uemura T, Maeda A, Shiroshima T, Iwasawa-Okamoto S, Mori H, Mishina M, Fukui S. Mechanisms of splicing-dependent trans-synaptic adhesion by PTP δ -IL1RAPL1/IL-1RAcP for synaptic differentiation. *Nat Commun.* 2015;6:6926. Epub 2015/04/25. doi: 10.1038/ncomms7926. PubMed PMID: 25908590; PMCID: PMC4423211.
10. Barr AJ, Ugochukwu E, Lee WH, King ON, Filippakopoulos P, Alfano I, Savitsky P, Burgess-Brown NA, Müller S, Knapp S. Large-scale structural analysis of the

classical human protein tyrosine phosphatome. *Cell*. 2009;136(2):352-63. Epub 2009/01/27. doi: 10.1016/j.cell.2008.11.038. PubMed PMID: 19167335; PMCID: PMC2638020.

Chapter Four: Characterization of the Asprosin-PTPRD Interaction

Introduction

Since its initial discovery, asprosin has been implicated in several different signaling pathways operating within different tissues in the body including the liver, skeletal muscle cells, pancreatic β cells, and our tissue of interest, hypothalamic neurons (1). In the pancreas, asprosin interacts with TLR4 to cause an overall effect of decreasing insulin production and increasing inflammation (2). In the liver, asprosin interacts with the G-protein coupled receptor OLF734, having an overall effect of increasing hepatic glucose release (3).

Initial studies of asprosin revealed that asprosin's interaction in the brain had the effect of increasing AgRP neuronal activity, which in-turn stimulated appetite. It was predicted that asprosin was working through a G-protein coupled receptor because injections of asprosin in mice caused an increase in cyclic adenosine monophosphate (cAMP), which is a consistent phenomenon observed with G-protein coupled receptors that couple to protein $G_{\alpha s}$ (4). However, a recent study identified protein tyrosine phosphatase receptor type D (PTPRD) as the receptor in the hypothalamus responsible for appetite stimulation through the asprosin interaction (5). PTPRD was identified as asprosin's receptor by homogenizing mice brains and incubating the homogenate with asprosin. This incubation was followed by an asprosin immunoprecipitation and mass spectrometry analysis yielding 58 interactors, of these interactors, PTPRD was the only membrane-bound receptor (5). The binding affinity of asprosin and PTPRD was then quantified using micro-scale thermophoresis, bio-layer interferometry, and surface plasmon resonance, which all measured a K_D in the low nanomolar range, indicating a strong affinity for the interaction (5).

While previous work has validated this interaction both biochemically and *in vivo*, there has not been any structural characterization done for the asprosin-PTPRD complex. One of the main goals for my project was to use cryogenic electron microscopy (cryo-EM) to define the asprosin-PTPRD binding interface. Defining the binding interface would enable pharmacologic design to aid in the treatment of obesity through appetite modulation. Structural characterization of the asprosin-PTPRD will also be validated with biochemical assays.

Results

Negative Stain Electron Microscopy

I used negative stain electron-microscopy (NS-EM) to characterize asprosin in complex with full length PTPRD extracellular domain to obtain initial information on the structural organization of this complex. A complex of PTPRD extracellular domain, purchased for initial screening, and asprosin was made by combining 3 μM of each protein followed by dilution to 0.015 μM in phosphate buffer solution, to give an optimal protein distribution for visualization. The grid was stained with 0.75% uranyl formate and was visualized using a FEI Talos 120 KV (TEM) equipped with LaB6 and 4k Ceta detector (ThermoFisher Scientific). Eighty images were collected and processed through CTF correction, particle picking, particle extraction, and 2D classifications. A Y-shaped complex, with two long arms was visible following iterative rounds of 2D classification (**Fig. 4.1**). Grids with PTPRD alone were prepared using the same protocol as previously described, and no Y-shaped complex was visible, indicating the structure observed is likely dependent on asprosin binding at such low concentrations.

Cryogenic Electron Microscopy

Following the promising low-resolution negative stain data, we decided to push forward with cryo-EM, in hopes that we would be able to obtain higher resolution data. For initial screening, I began by incubating a 3 μM complex of both asprosin and PTPRD. I diluted the complex to 0.3 μM and 0.6 μM following incubation. For initial screening purposes, I used c-flat grids. I chose c-flat as this is a good option for the thinnest ice formation when vitrifying. Gold is a good choice when working with smaller proteins as it allows for highest resolution data collection. Grids were vitrified in liquid ethane using a Vitrobot IV (ThermoFisher Scientific).

Following grid preparation, grids were viewed, and data was collected using a FEI Artica 200 KV (TEM) equipped with LaB6 and 4k Ceta detector (ThermoFisher Scientific). Images were acquired using a nominal magnification of 92,000X at a pixel size of 0.84 Å and a dose of 37.6 e⁻/s. Five-hundred twenty-four images were collected and processed in Cryosparc 2.2 (6) for CTF correction, particle picking, particle extraction, and 2D classifications. 2D classification revealed that the complex has dissociated on the grids. No asprosin-PTPRD complex was visible in the images collected (**Fig. 4.2**).

Bio-Layer Interferometry

The interaction between asprosin and PTPRD had previously been characterized biochemically by the Chopra lab using bio-layer interferometry (BLI). To ensure that the protocol used by the Chopra lab was optimal using our system, I began by replicating and validating the experiment. PTPRD contains a multi-domain extracellular domain, and it is unclear which domains are responsible or necessary for the asprosin interaction. I previously described expression and purification strategies of different domains of PTPRD. These truncated PTPRD domains are intended to be used in biochemical assays

to aid in elucidating the necessary PTPRD components for asprosin binding. BLI was used to determine which domain of PTPRD directly interacts with asprosin. I biotinylated purified PTPRD domains using an EZ-Link Sulfo-NHS-Biotinylation kit, which adds biotin to the primary amines present in each protein. This enabled individual PTPRD domains to be conjugated to a streptavidin biosensor. The binding affinities for asprosin with individual PTPRD domains were measured using an Octet BLI system. Five different concentrations of each protein were measured. The Chopra lab reported the K_D of asprosin and the full-length extracellular domain of PTPRD as 57.0 nM. Following the same method, I measured the K_D of asprosin and the full-length extracellular domain of PTPRD as 24.2 nM (**Fig. 4.3**). The K_D of asprosin and PTPRD-IgG the K_D of asprosin and PTPRD-Fn were not able to be derived because the traces associated with the individual PTPRD domains (Fn and IgG) showed some irregularities and did not have a clean measured on-rate and off-rate. This was a phenomenon observed several times.

Discussion

Negative stain EM data for grids with asprosin and full-length extracellular domain of PTPRD revealed formation Y-shaped complex, with two long arms. A control with PTPRD alone contained no visible Y-shaped complex, indicating the structure observed is likely dependent on asprosin binding at such low concentrations. These data lead me to hypothesize that binding to asprosin may enhance PTPRD dimerization, which is consistent with the canonical oligomerization of PTP family proteins. I also hypothesize that asprosin is binding to the shorter IgG domain of PTPRD and the arms of the structure are formed from the longer, unbound Fn domains. It is still desirable to obtain higher resolution structural information using cryo-EM. Cryo-EM conditions for this complex need to be optimized, which is a challenge as each component of the complex is difficult to

obtain, and greater concentrations of protein may be necessary in order to identify optimal grid conditions. I initially chose to screen the complex on c-flat grids, as vitreous ice tends to form in the thinnest layer on this type of grid, which can help with visualizing smaller complexes. Thinner ice also enables higher resolution data to be collected. While this was sound rationale to screen with c-flat grids, it may be a good idea to begin screening the asprosin-PTPRD complex using different types of grids, such as holey carbon, lacey carbon or gold grids. Since complex dissociation during vitrification is the most relevant issue that prevents us from proceeding forward, it is important to optimize conditions to have the smallest amount of background components (either unbound asprosin or unbound PTPRD). A way to minimize this background would be to complex asprosin and PTPRD and then use size-exclusion chromatography to separate out complex from protein aggregates and unbound proteins. However, this option has not been able to be explored up to this point because it requires significantly higher concentrations of the proteins to be used, and protein amounts have not been sufficient to explore this option.

I was successfully able to replicate the BLI experiment done by the Chopra lab, which was an important first step in my domain mapping experiment. This enabled me to be confident in the K_D values associated with the binding events of each individual PTPRD domain with asprosin. Binding experiments with each PTPRD domain did not indicate a difference in binding between the PTPRD-IgG domains and the PTPRD-Fn domains. However, the reliability of this derived K_D is confounded by the irregularities observed in the traces for the individual PTPRD domains. This result may be due to the non-specific nature in which the PTPRD domains were biotinylated. Another binding assay method should be used to validate the observations from BLI. Surface plasmon resonance (SPR)

may be another good method to use as it is even more sensitive than BLI. It may also be beneficial to switch which protein is conjugated to the biosensor, to mitigate the possibility that conjugation of protein to the biosensor could cause a change in binding kinetics. For my experiments I biotinylated each PTPRD domain and conjugated them to the streptavidin biosensor. It may be better to biotinylate and conjugate asprosin instead. This may be a more strategic design as the same exact protein will be conjugated to the biosensor, and changes in binding kinetics can be attributed directly to differences in interactions between asprosin and each PTPRD domain. However, this requires significantly more asprosin to be used in the assay, which is not obtainable with the amount of asprosin that we currently have. Another consideration could be to use a specific method of biotinylation, such as incorporation of an Avi tag into each of the PTPRD constructs. While the EZ-Link Sulfo-NHS-Biotinylation kit is an effective way to biotinylate each protein, it does introduce heterogeneity to the sample, which can effect binding results.

Figures

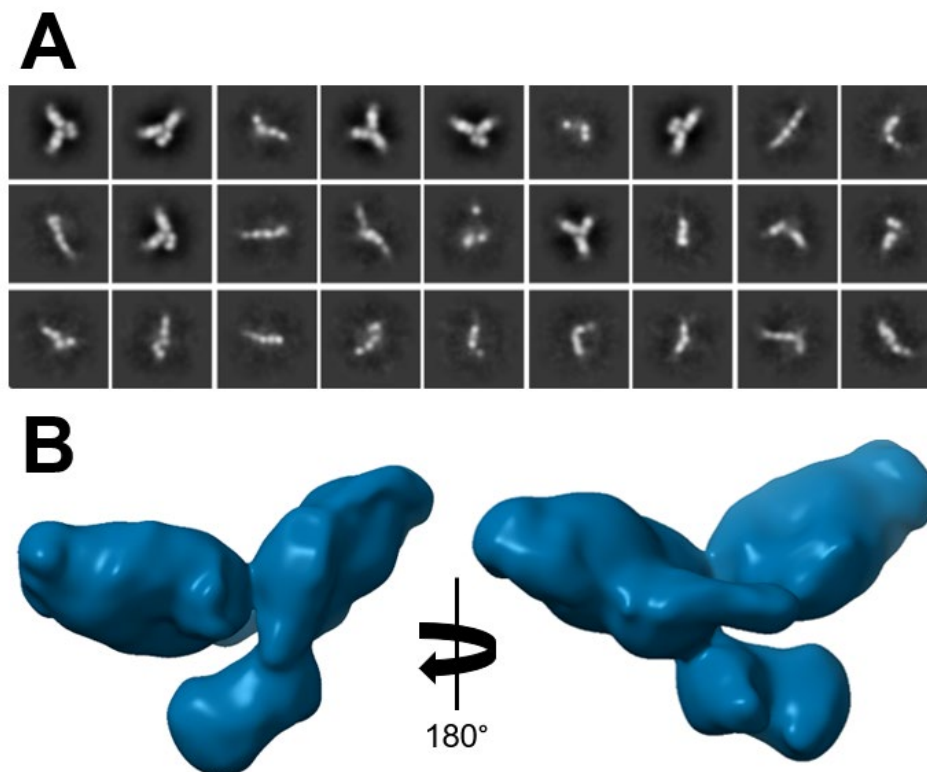


Figure 4.1: Reconstruction of the PTPRD-asprosin complex by negative-stain EM. **A)** Reference free 2D classes derived from the negative stain data. **B)** 3D reconstruction of asprosin-PTPRD generated from 2D classes of panel B. The asprosin-PTPRD complex forms a y-shaped complex. These data suggest that PTPRD interacts with asprosin as a dimer.

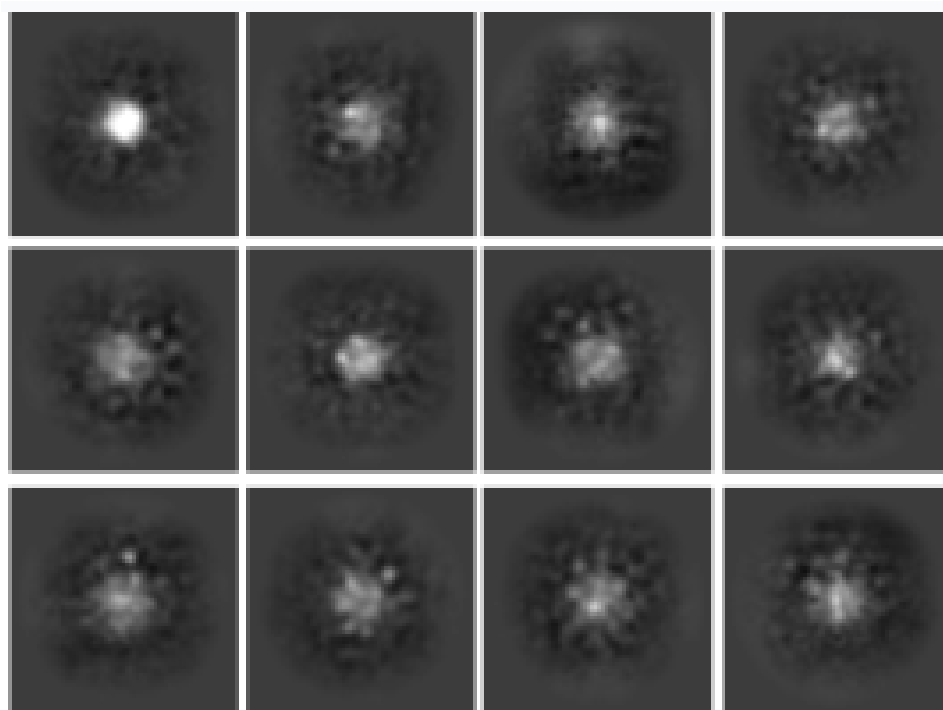
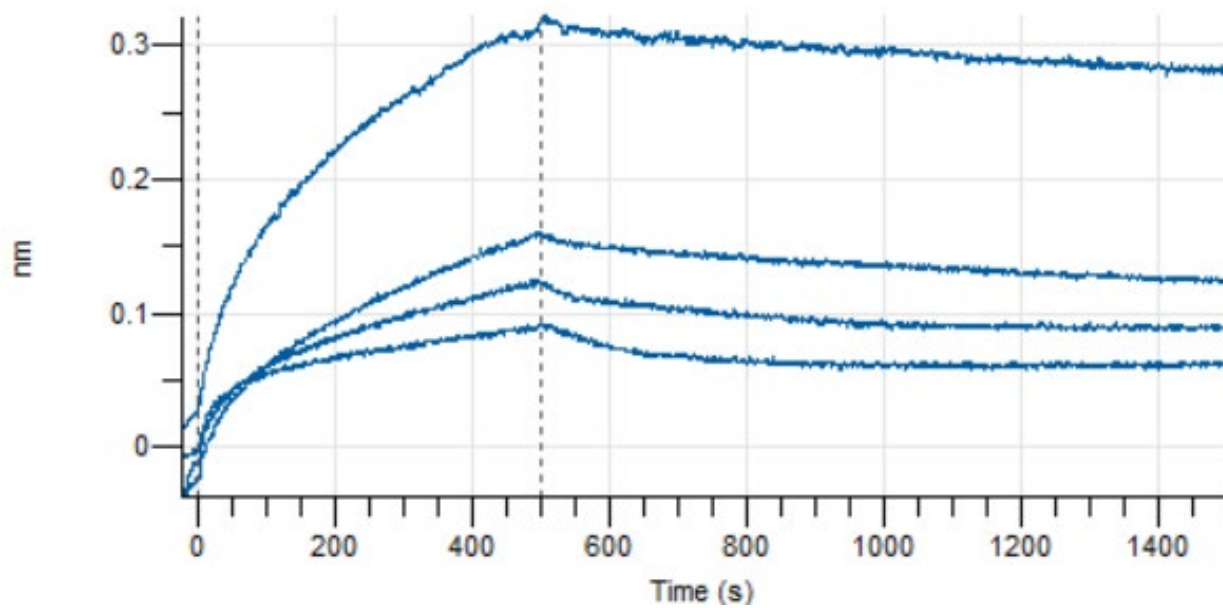


Figure 4.2: 2D Classes of the Asprosin-PTPRD Complex. Reference-free 2D classes derived from cryo-EM data. These data do not show a defined shape of the asprosin-PTPRD complex, likely due to dissociation of the complex during vitrification.



KD (M)	KD Error	ka (1/Ms)	ka Error	kdis (1/s)	RSS	Full R ²
2.423E-08	2.664E-10	7.391E03	4.136E01	1.791E-04	5.9037	0.9736

Figure 4.3: Binding Kinetics of Asprosin and full-length extracellular domain of PTPRD Determined Using BLI. The measured K_D of the asprosin-full-length PTPRD interaction is 24.2 nM.

Methods/Materials

Negative Stain Electron Microscopy

A complex of PTPRD extracellular domain (ACROBiosystems, Human PTPRD Protein, His-Tag), and asprosin (Biolegend, Recombinant Human Asprosin (Carrier-Free)) was made by combining 3 μM of each protein followed by dilution to 0.015 μM in phosphate buffer solution, to give an optimal protein distribution for visualization. Grids were glow-discharged (PELCO easiGLOW). The grid was stained with 0.75% uranyl formate and was visualized using a FEI Talos 120 KV (TEM) equipped with LaB6 and 4k Ceta detector (ThermoFisher Scientific). Images were acquired using a nominal magnification of 92,000X at a pixel size of 1.57Å and a dose of 50 e⁻/s . Eighty images were collected and processed in Cryosparc 2.2 (6) for CTF correction, particle picking, particle extraction, and 2D classifications.

Cryogenic Electron Microscopy

A complex of PTPRD extracellular domain (ACROBiosystems, Human PTPRD Protein, His-Tag), and asprosin (Biolegend, Recombinant Human Asprosin (Carrier-Free)) was made by combining 3 μM of each protein. The complex was incubated for one hour at 4 °C. Following incubation, the complex was diluted to 0.3 μM and 0.6 μM . Three microliters of the complex were applied onto a freshly glow-discharged (PELCO easiGLOW) 400-mesh, 1.2/1.3 C-Flat grid (Electron Microscopy Sciences). After 20 s of incubation, grids were blotted for 3 s at 0 blot force and vitrified using a Vitrobot IV (ThermoFisher Scientific) under 22°C with 100% humidity. Grids were viewed and data was collected using a using a FEI Artica 200 KV (TEM) equipped with LaB6 and 4k Ceta detector (ThermoFisher Scientific). Images were acquired using a nominal magnification of 92,000X at a pixel size of 0.84 Å and a dose of 37.6 e⁻/s. Five-hundred twenty-four images were collected and

processed in Cryosparc 2.2 (6) for CTF correction, particle picking, particle extraction, and 2D classifications.

Bio-Layer Interferometry

The binding affinity of asprosin to PTPRD was measured on Sartorius Octet RED96 system. The PTPRD protein (ACROBiosystems, Human PTPRD Protein, His-tag) was labeled with Biotin using EZ-Link-Sulfo-NHS-Biotin (ThermoFisher Scientific, 21217) and desalted by Zeba™ Spin Desalting Columns. The biotin-labeled PTPRD (20µg/ml) was loaded on streptavidin biosensors for 300 seconds. Following 20 seconds of baseline in kinetics buffer (PBS + 0.1% BSA, 0.02% Tween20 and Kathon). The loaded biosensors were dipped into a series of 5-fold human asprosin (3.125–25 µg/mL) for 300 seconds to record association kinetics and then dipped into a kinetic buffer for 600 seconds to record dissociation kinetics. Kinetic buffer without asprosin was set to correct the background. For fitting of KD value, ForteBio's data analysis software was used to fit the curve by a 1:1 binding model and the global fitting method was applied. The same procedure was used for each PTPRD domain (PTPRD-IgG and PTPRD-Fn).

References

1. Yuan M, Li W, Zhu Y, Yu B, Wu J. Asprosin: A Novel Player in Metabolic Diseases. *Frontiers in Endocrinology*. 2020;11. doi: 10.3389/fendo.2020.00064.
2. Lee T, Yun S, Jeong JH, Jung TW. Asprosin impairs insulin secretion in response to glucose and viability through TLR4/JNK-mediated inflammation. *Mol Cell Endocrinol*. 2019;486:96-104. Epub 2019/03/12. doi: 10.1016/j.mce.2019.03.001. PubMed PMID: 30853600.
3. Li E, Shan H, Chen L, Long A, Zhang Y, Liu Y, Jia L, Wei F, Han J, Li T, Liu X, Deng H, Wang Y. OLF734 Mediates Glucose Metabolism as a Receptor of Asprosin. *Cell Metab*. 2019;30(2):319-28.e8. Epub 2019/06/25. doi: 10.1016/j.cmet.2019.05.022. PubMed PMID: 31230984.
4. Duerschmid C, He Y, Wang C, Li C, Bournat JC, Romere C, Saha PK, Lee ME, Phillips KJ, Jain M, Jia P, Zhao Z, Farias M, Wu Q, Milewicz DM, Sutton VR, Moore DD, Butte NF, Krashes MJ, Xu Y, Chopra AR. Asprosin is a centrally acting orexigenic hormone. *Nat Med*. 2017;23(12):1444-53. Epub 2017/11/07. doi: 10.1038/nm.4432. PubMed PMID: 29106398; PMCID: PMC5720914.
5. Mishra I, Xie WR, Bournat JC, He Y, Wang C, Silva ES, Liu H, Ku Z, Chen Y, Erokwu BO, Jia P, Zhao Z, An Z, Flask CA, He Y, Xu Y, Chopra AR. Protein tyrosine phosphatase receptor δ serves as the orexigenic asprosin receptor. *Cell Metab*. 2022;34(4):549-63.e8. Epub 2022/03/18. doi: 10.1016/j.cmet.2022.02.012. PubMed PMID: 35298903; PMCID: PMC8986618.
6. Asarnow D, Palovcak, E., Cheng, Y. UCSF pyem v0.5. Zenodo2019. doi: 0.5281/zenodo.3576630.

Chapter Five: Future Considerations for the Asprosin Project

While efforts up to this point have not yielded successful methodology for the issue of expression and purification of asprosin and PTPRD, there are strategic next steps that can be taken to make progress despite these issues. The avenues discussed in this chapter are directions in which this project can be taken to make progress towards characterizing asprosin's interaction with PTPRD.

Deep Mutational Scanning

Due to the incredible challenges associated with expression and purification of both asprosin and PTPRD, it is possible that a non-structural approach will need to be taken to elucidate the binding interface between asprosin and PTPRD. A logical approach would be to use a mammalian surface-display platform and deep mutational scanning. This is an approach that has been used by the Ortlund lab previously in its investigation of important mutations of nucleocapsid protein in SARS-CoV-2 (1). Deep mutational scanning is a high-throughput method in which a library of possible mutations in a protein is generated. This library can contain thousands of unique sequences, in which each amino acid residue in a protein is mutated to each possible amino acid. Mutations generated in this library can be used for functional assays, to determine which residues in a given protein are important for specific functions. Specifically for the asprosin project, a library could be generated to contain every possible mutation of asprosin. Individually, these mutations could be tested for binding with PTPRD, or any other interacting partner of asprosin. If binding to PTPRD is lost following mutation of certain residues, we will be able to identify important residues for the interaction.

Site-Directed Mutagenesis

Aside from identifying mutations that can be made to asprosin through deep mutational scanning, I have already identified some amino acid residues that I hypothesize are important for PTPRD binding. I began to identify these residues by investigating other interacting partners of PTPRD and where they interact with PTPRD. I initially hypothesized that asprosin would bind somewhere between the Ig3 and Fn2 domains of the extracellular portion of PTPRD. This seemed like a promising region because this is where PTPRD's mini-exon (Me) peptides are located, which have been thought to confer PTPRD binding specificity. As mentioned in previous chapters, PTPRD has been crystallized with its interacting partners, interleukin-1 receptor accessory protein (IL-1RAcP) and IL-1RAcP-like-1 (IL1RAPL1) (2). IL-1RAcP and IL1RAPL1 are multi-domain proteins that are structurally comprised of multiple Ig-folds. The structure of asprosin, as predicted by AlphaFold is also comprised of an Ig-fold. Due to this similarity in organizational structure between PTPRD's binding partners, I decided to overlay the crystalized structure of IL1RAPL1 with asprosin. The two proteins overlaid well and had very similar structures at the region in which IL1RAPL1 is known to bind to PTPRD. I took the amino acid sequence of this region of mouse and human IL1RAPL1 and did a multiple-sequence alignment with the amino acid sequences of human asprosin (**Figure 5.1**). I found two regions in which asprosin and IL1RAPL1 and asprosin shared common amino acid sequence and predicted structural similarities. Since biochemical characterization of asprosin and PTPRD has been well established through the Chopra lab with BLI, SPR, and MST, it is my suggestion that the identified amino acid residues be mutated on asprosin and tested using these biochemical assays. If mutation of these residues leads to loss of PTPRD binding in functional assays, we can determine that

these residues were important for binding. The residues that I suggest mutating in asprosin are E28 and G67.

Asprosin Clinical Trial

In collaboration with the Marcus Autism Center, the Ortlund lab is participating in a clinical trial that will measure plasma levels of asprosin in patients diagnosed with pediatric feeding disorders (PFD). PFD significantly impacts the quality of life in patients and is very prevalent, affecting 1 in 23 to 1 in 37 of all children under the age of five (3). PFD is described as being the inability to consume age-appropriate foods that provide full nutritional needs. There are a variety of causes for PFD including dysfunction of neurologic (e.g., cerebral palsy), gastrointestinal, cardiorespiratory (e.g. congenital cardiac disease or stroke), and neurobehavioral conditions (e.g. autism) and puts children at great medical, nutritional, feeding skill, and psychosocial risk. The goal of the study is to use metabolomics to profile differences in metabolites based off of severity of feeding disorders. Additionally, asprosin levels will be monitored to describe associations of levels with potential covariates (such as age, gender, and medical/behavioral conditions). A sandwich ELISA, developed by the Chopra lab, will be used as the method of detection **(Figure 5.2)** (4).

Placensin and Gonascin

Asprosin is the c-terminal cleavage product of the FBN1 gene. However, there are two additional FBN genes, FBN2 and FBN3, which also contain c-terminal products similar in size to asprosin. The cleavage product of FBN2 is known as placensin and has been found to be secreted from the human placenta (5). Similarly to asprosin, placensin was shown to have glucogenic effects on mice following tail vein injection. Additionally,

placensin was able to be expressed and purified from *E. coli* (5). The cleavage product of FBN3 has yet to be characterized, but is referred to as gonascin. AlphaFold modeling has revealed that the cleavage products of FBN2 and FBN3 are also Ig-folds, similar to asprosin. It is important to determine the physiological effects that these cleavage products have, and if they share the same function and target tissues as asprosin. Specifically, if placensin is able to interact with PTPRD in the hypothalamus in the same way as asprosin this could provide helpful information about the asprosin-PTPRD interaction. Since placensin is able to be expressed bacterially, and the predicted structure is similar to asprosin, structural studies with placensin and PTPRD could provide insight on the interaction between asprosin and PTPRD. Additionally, studying the differences between asprosin and placensin could aid in designing a construct of asprosin that is more readily expressed in bacteria. Characterization of all three cleavage products would give a holistic picture of the role that the FBN genes play in metabolism and energy regulation. This understanding would enable more efficient design of pharmacological compounds that could target the asprosin-PTPRD interaction for treatment of obesity through appetite modulation.

Figures

```

Asprosin          -----STNETDASDIQDGSEMEANVSLASWDVEKPASFAFNISHVNNKVRILELLPAL      53
IL1RAPL1[Mouse]  PHLILLYATFTQS---LKVVTKRGSADGCTDWSVDIKKYQVL----VGEPVRIKC-----      48
IL1RAPL1[Human]  -----LKVVTKRGSADGCTDWSIDIKKYQVL----VGEPVRIKC-----      35
                  ::  ::  :  .  .  *  .  :  :  .  :  *  .  :  *  *  *

Asprosin          TTLMNHRYLIESGNEDGFFKINQKEGVSYLHFTKKKPVAGTYSLQISSTPL-----Y      106
IL1RAPL1[Mouse]  -----ALFYGYIRTNYSLAQSAGLSLMWYKSSGPGDFEPIAFDGSRMSKEEDSIW      99
IL1RAPL1[Human]  -----ALFYGYIRTNYSLAQSAGLSLMWYKSSGPGDFEPIAFDGSRMSKEEDSIW      86
                  :  *  :  .  :  *  *  *  :  :  .  .  *  :  :  .  .  :  :

Asprosin          KKKELNQLEDRYDKDYLSGELGDNLKMKIQILLH 140
IL1RAPL1[Mouse]  FRPTLLQDSGLYAC---VIRNSTYCMKVSISLT 129
IL1RAPL1[Human]  FRPTLLQDSGLYAC---VIRNSTYCMKVSISLT 116
                  :  *  *  .  .  *  .  .  .  *  *  :  *  *

```

Figure 5.1: Multiple sequence alignment of asprosin and IL1RAPL1. Comparison of primary amino acid sequences for asprosin, IL1RAPL1 (mouse), and IL1RAPL1 (human). The residues of mouse IL1RAPL1 that interact directly with PTPRD are highlighted in yellow. Conserved residues are annotated by (*) for identical residues, (:) for conserved substitutions, and (.) for semi-conserved substitutions. Of the residues that interact directly with PTPRD, E28 and G67 are conserved in asprosin.

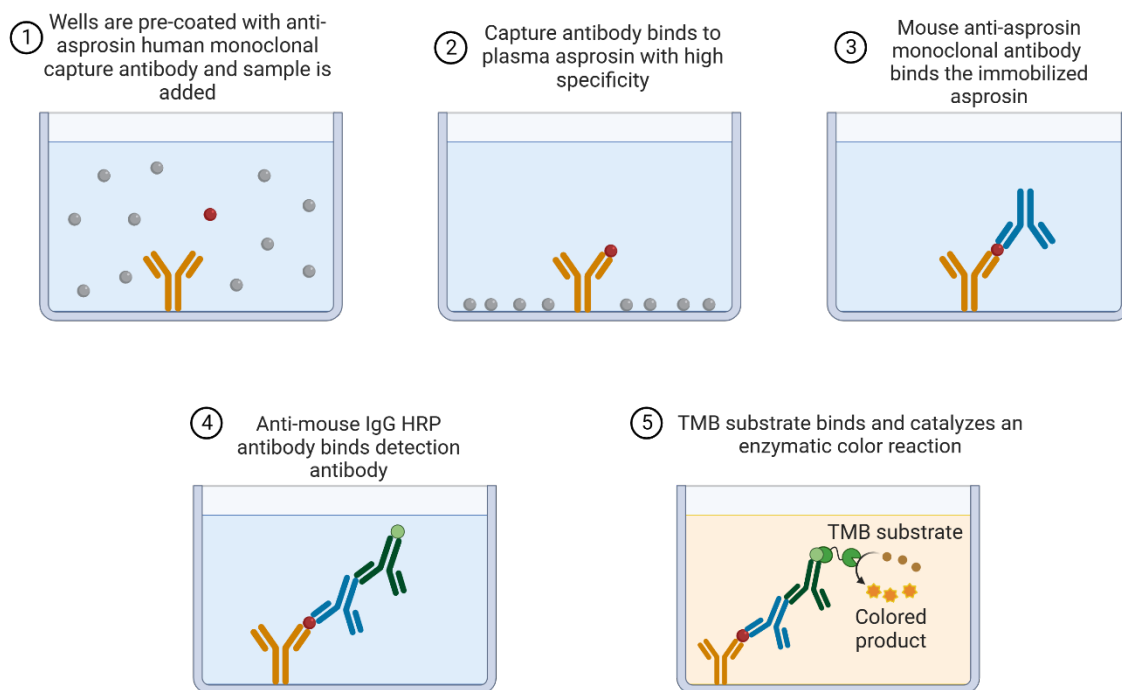


Figure 5.2: Sandwich ELISA used for plasma asprosin detection. Plasma levels of asprosin in patients with pediatric feeding disorders will be measured to describe association of levels with co-variates. Figure created using BioRender.

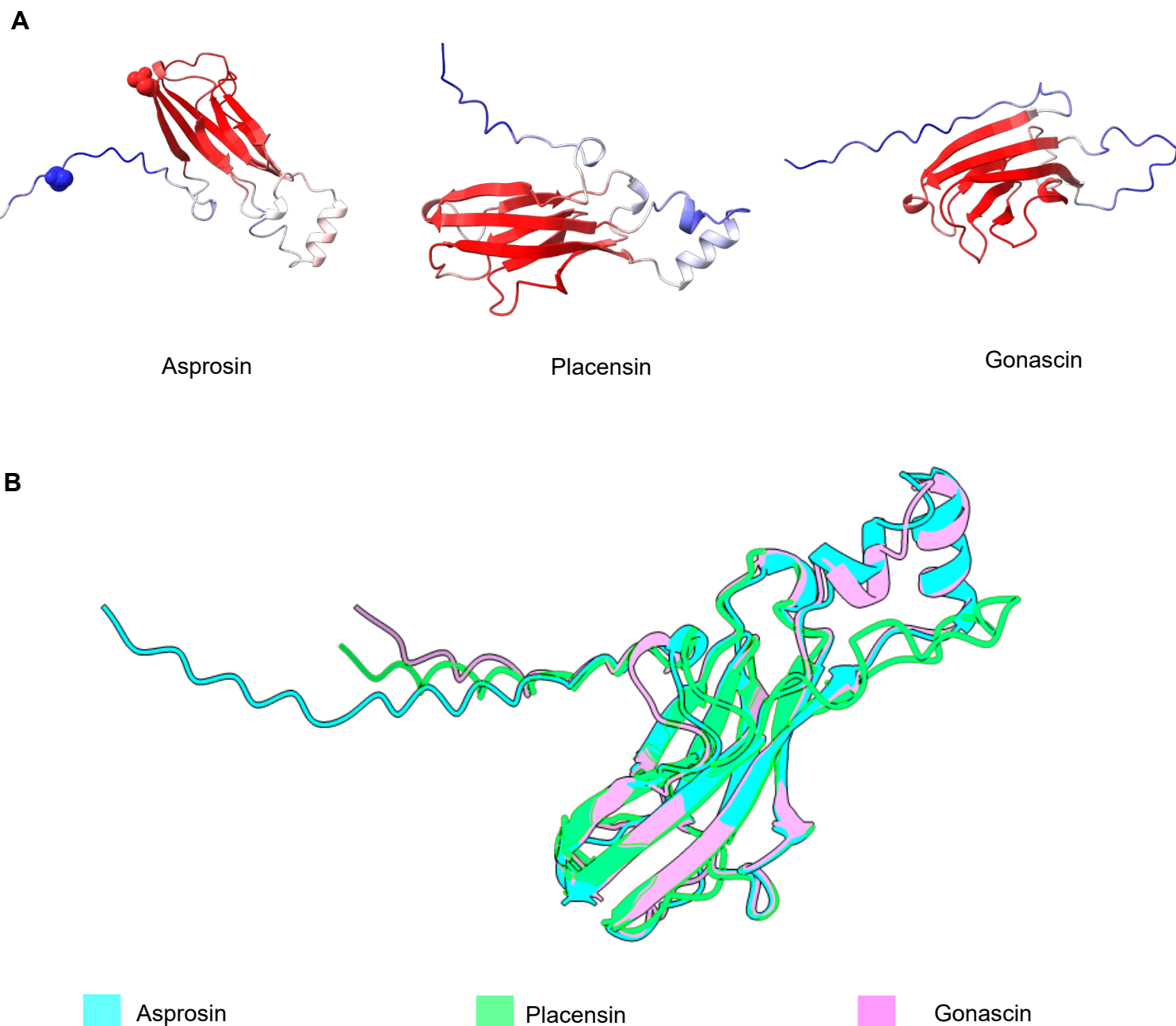


Figure 5.3: 3D modeling of asprosin, placensin, and gonascin. A) AlphaFold predictions of the structures of asprosin, placensin, and gonascin. Each model is colored by confidence, with red being areas of high confidence, and blue being low confidence. B) Overlay of predicted structures. While the primary amino acid sequence of the proteins vary greatly, they share a similar overall structure. Asprosin is in cyan, placensin in green and gonascin in pink.

References

1. Frank F, Keen MM, Rao A, Bassit L, Liu X, Bowers HB, Patel AB, Cato ML, Sullivan JA, Greenleaf M, Piantadosi A, Lam WA, Hudson WH, Ortlund EA. Deep mutational scanning identifies SARS-CoV-2 Nucleocapsid escape mutations of currently available rapid antigen tests. *Cell*. 2022;185(19):3603-16.e13. Epub 2022/09/10. doi: 10.1016/j.cell.2022.08.010. PubMed PMID: 36084631; PMCID: PMC9420710.
2. Yamagata A, Yoshida T, Sato Y, Goto-Ito S, Uemura T, Maeda A, Shiroshima T, Iwasawa-Okamoto S, Mori H, Mishina M, Fukai S. Mechanisms of splicing-dependent trans-synaptic adhesion by PTP δ -IL1RAPL1/IL-1RAcP for synaptic differentiation. *Nature Communications*. 2015;6(1):6926. doi: 10.1038/ncomms7926.
3. Kovacic K, Rein LE, Szabo A, Kommareddy S, Bhagavatula P, Goday PS. Pediatric Feeding Disorder: A Nationwide Prevalence Study. *J Pediatr*. 2021;228:126-31.e3. Epub 2020/07/24. doi: 10.1016/j.jpeds.2020.07.047. PubMed PMID: 32702429.
4. Mishra I, Chopra AR. Overexpression and ELISA-based detection of asprosin in cultured cells and mice. *STAR Protoc*. 2022;3(4):101762. Epub 2022/10/15. doi: 10.1016/j.xpro.2022.101762. PubMed PMID: 36240062; PMCID: PMC9568886.
5. Yu Y, He JH, Hu LL, Jiang LL, Fang L, Yao GD, Wang SJ, Yang Q, Guo Y, Liu L, Shang T, Sato Y, Kawamura K, Hsueh AJ, Sun YP. Placensin is a glucogenic hormone secreted by human placenta. *EMBO Rep*. 2020;21(6):e49530. Epub 2020/04/25. doi: 10.15252/embr.201949530. PubMed PMID: 32329225; PMCID: PMC7271319.